



SCHOOL of
GRADUATE STUDIES
EAST TENNESSEE STATE UNIVERSITY

East Tennessee State University
**Digital Commons @ East
Tennessee State University**

Electronic Theses and Dissertations

Student Works

12-2010

High Impedance Arc Fault Detection in a Manhole Environment.

Thomas Arthur Cooke
East Tennessee State University

Follow this and additional works at: <https://dc.etsu.edu/etd>



Part of the [Electrical and Electronics Commons](#)

Recommended Citation

Cooke, Thomas Arthur, "High Impedance Arc Fault Detection in a Manhole Environment." (2010). *Electronic Theses and Dissertations*. Paper 1767. <https://dc.etsu.edu/etd/1767>

This Thesis - Open Access is brought to you for free and open access by the Student Works at Digital Commons @ East Tennessee State University. It has been accepted for inclusion in Electronic Theses and Dissertations by an authorized administrator of Digital Commons @ East Tennessee State University. For more information, please contact digilib@etsu.edu.

High Impedance Arc Fault Detection in a Manhole Environment

A thesis

presented to

the faculty of the Department of Engineering Technology

East Tennessee State University

In partial fulfillment

of the requirements of the degree

Master of Science in Technology

by

Thomas Arthur Cooke

December 2010

Joseph P. Sims, Chair

Keith V. Johnson

William A. Clark

Hugh W. Broome

Keywords: Arc Detection, High Impedance Fault, Incipient Fault, Arcing Algorithm

ABSTRACT

High Impedance Arc Fault Detection in a Manhole Environment

by

Thomas Arthur Cooke

The scope of this thesis was to develop a prototype high-impedance arc detection system that a utility worker could use as an early warning system while working in a manhole environment. As part of this system sensors and algorithms were developed to increase the sensitivity of detecting an arc while ignoring loads that can give false positive signatures for arcing. The latest technology was used to repeat measurements performed in previous research from decades ago that lacked in sampling speed and amplitude resolution. Several types of arcs were produced and analyzed so to establish a library of various waveform and frequency signatures. The system was constructed as a development unit and is currently gathering information in the field. Data being collected will be analyzed so future revisions will give higher confidence levels of arc detection. Other future plans involve designing a more compact and portable unit.

Copyright 2010 by Thomas A. Cooke

All Rights Reserved

DEDICATION

This thesis is dedicated to my wife and children who have tolerated my absence from many family occasions while I pursue my education. To my parents, thanks for your guidance and support in life.

“Whoso loveth instruction loveth knowledge:
but he that hateth reproof is brutish.”

(Proverbs 12:1)

ACKNOWLEDGEMENTS

I would like to thank Dr. Paul Sims for standing as my Committee Chair and the rest of the Advisory Committee, Dr. Johnson, Dr. Clark, and Mr. Hugh Broome for their support. Special thanks to the Department of Technology and their staff at ETSU for supporting a remote campus site in Knoxville, Tennessee. Your service has given me a more efficient opportunity to continue my education while balancing my work and family life.

I would like to thank all my colleagues at the Electric Power Research Institute for years of on-the-job learning and experience. For this project I especially want to thank Doug Dorr and Kermit Phipps for their guidance and support. I would also like to thank EPRI management for encouragement and support in continuing education.

CONTENTS

	Page
ABSTRACT	2
LIST OF TABLES	9
LIST OF FIGURES	10
Chapter	
1. INTRODUCTION	13
Problem Statement	14
2. LITERATURE REVIEW	16
3. METHODS	19
Electrical Distribution Manhole Environment	19
Sensor Selection	20
Optical Sensors	20
Temperature Sensors	20
Pressure Sensors	20
Direct Voltage and Current Sensors	21
Magnetic Field Sensor	21
RF Electric Field Sensor	21
Sensor Development	22
Magnetic Field Sensor	22
Electric Field Sensor	23
Arcing Analysis	28

Data Acquisition for Analysis.....	28
Arc Characterization	29
Carbon Rod Arcing Waveform Analysis	29
Crest Factor.....	31
Differentiation.....	32
Carbon Rod Frequency Analysis.	33
Sand Slurry Arc Source	35
Sand Slurry Arcing Waveform Analysis.	35
Sand Slurry Arcing Frequency Analysis.....	36
Manhole Arcing Simulation with Contaminants	37
E-Field Data Analysis	40
Potential False Positives	42
Algorithm Development	46
H-Field Algorithm	46
E-Field Algorithm.....	48
Alarm Decision Logic.....	49
Digital Signal Processing.....	50
Design	51
4. RESULTS AND DISCUSSION.....	53
Lab Testing	54
Crest Factor Algorithm Results	57
Differentiation Algorithm Results	58
Interharmonics Algorithm Results	59

120 Hz Repetition Algorithm Results.....	60
120 Hz Demodulation Algorithm Results.....	61
180 Hz Demodulation Algorithm Results.....	62
Sporadic Efield Algorithm Result.....	63
Field Testing	64
5. CONCLUSION.....	66
Future Recommendations	66
REFERENCES	68
APPENDIX: Series Sequence of Waveforms from a Single Arcing Event	70
VITA.....	77

LIST OF TABLES

Table	Page
1. Summary of Detection Methods from Literature Review	17
2. Summary of Parameters and Algorithms from Literature Review	18

LIST OF FIGURES

Figure	Page
1. Illustration of Proposed use of Arc Detection System.....	14
2. Typical Electrical Distribution Manhole Environment.....	19
3. Common Magnetic Field Antennas	23
4. Illustration of How an AM Radio Detects Arcing.....	24
5. Illustration of Field Test Setup to Measure Radio Frequencies in a Manhole.....	26
6. RFI Locator Indicating when Arcing is Present	27
7. Selected E-Field Detection Unit for Arc Detection System	27
8. Instrumentation used for Arc Characterization.....	29
9. Carbon Rod Arc Generator	29
10. Typical Current and E-Field Meter Output from Carbon Rod Arc Generator	30
11. Current and E-Field Output with Minimized Air Gap between Carbon Rods	31
12. Analysis of a Perfect Sine Wave Versus an Arcing Waveform using Crest Factor	32
13. Differentiation of an Arcing Waveform	33
14. Frequency Analysis of Carbon Rod Arcing.....	34
15. High Frequency Analysis of Carbon Rod Arcing.....	34
16. Sand Slurry Arc Generator.....	35
17. Varying Waveforms Produced from Sand Slurry Arc Generator	36
18. Frequency Analysis of Sand Slurry Arc Generator	37
19. Conductors with Compromised Cuts to Simulate Contamination Process.....	38
20. Damage to Conductor Due to Compromised Cuts and Contamination.....	39

21. Current Waveform and E-Field Output from Sand Slurry Arcing	40
22. Frequency Analysis of E-Field Meter Output during Sand Slurry Arcing	41
23. Output Comparison of an AM Radio and E-Field Meter	42
24. Common Waveforms that Generate High Crest Factor as a False Positive for Arcing....	43
25. Neon Sign Current and Differentiation False Positive for Arcing.....	44
26. Frequency Analysis of E-Field Output Sensing DC Arcing from a Drill.....	45
27. Magnetic Field (H-Field) Algorithm Set	47
28. Electric Field (E-Field) Algorithm Set	49
29. Three Level Alarm Logic Diagram.....	49
30. CompactRIO™ Digital Signal Processor with LabView Screen Shots.....	50
31. Physical Inside Layout of Arc Detection System	51
32. Sensor Head Layout with H-Field and E-Field Antennas	52
33. The Manhole Arc Recognition System (M.A.R.S.).....	53
34. Lab Setup Simulating Manhole Ambient Currents with Arc Current	54
35. Baseline H-Field and E-Field Measurements from Lab Manhole Test	55
36. H-Field and E-Field Output from Arcing and False Positive Loads	56
37. Crest Factor Algorithm Test Results.....	57
38. Differentiation Algorithm Test Results	58
39. Interharmonics Algorithm Test Results	59
40. 120 Hz Repetition Rate Algorithm Test Results.....	60
41. 120 Hz Demodulation Algorithm Test Results.....	61
42. 180 Hz Demodulation Algorithm Test Results.....	62
43. Sporadic E-Field Algorithm Test Results.....	63

44. MARS System Used in a Field Environment 64

45. E-Field Frequency Analysis of Above Ground Subway with Arcing from DC Rail 65

46. Illustration of Future Goal for Smaller Hand-Held Arc Detection Unit..... 67

CHAPTER 1

INTRODUCTION

Manhole fires are very common in metropolitan cities. In a city like Washington DC with over 60,000 manholes over 90 of these events can occur each year. In New York City hundreds are reported each year. The most common cause stems from defects in the underground electrical distribution system that causes arcing. Couple that with accumulation of underground gases and you have a dangerous combination. Not only does this destroy the underground infrastructure, but for electrical workers who climb down in manholes to work on these power lines it can potentially create a lethal situation.

Currently workers take precautions such as measuring gas levels and pumping out any gases before entering the manhole. Even with these precautions, when pulling and tugging on wire whose insulation has been compromised can trigger an arc somewhere up or down stream in the electrical conduit. The burning of the insulation from the arc generated heat can generate deadly gases of its own. Carbon monoxide and combustible neoprene gas are just two that arise from the cables smoldering insulation. This arcing can start as a very subtle, high impedance arc. This means the resistance of the arc conduction path is high and will conduct small levels of current that will not open breakers or fuses upstream. The worker needs to have an indication that this is occurring to have an opportunity to exit the manhole before it escalates into a high-current, low impedance fault that can quickly fill the manhole with deadly smoke and gas.

To meet this need, as shown in Figure 1, a high impedance arc detection device is needed for the worker to use before entering and while working in a manhole. Even though arc detection research has been going on for decades, it has been proven to be a very complex process. The problem is not so much in detecting the arc, the problem is distinguishing it from

other signals that look like arcing. Many types of electrical loads can give false indications for arcing. With these false alarms, it's inevitable that workers become complacent and start ignoring any alarm altogether. This must be avoided by developing a system that produces the highest confidence that an arcing fault is occurring in their area. Currently, no such commercial apparatus exist to meet this need. The scope of this thesis is to build on this previous research by applying today's new technology and see if any advancements can be made with new sensors and algorithms to design and develop a manhole arc recognition system.

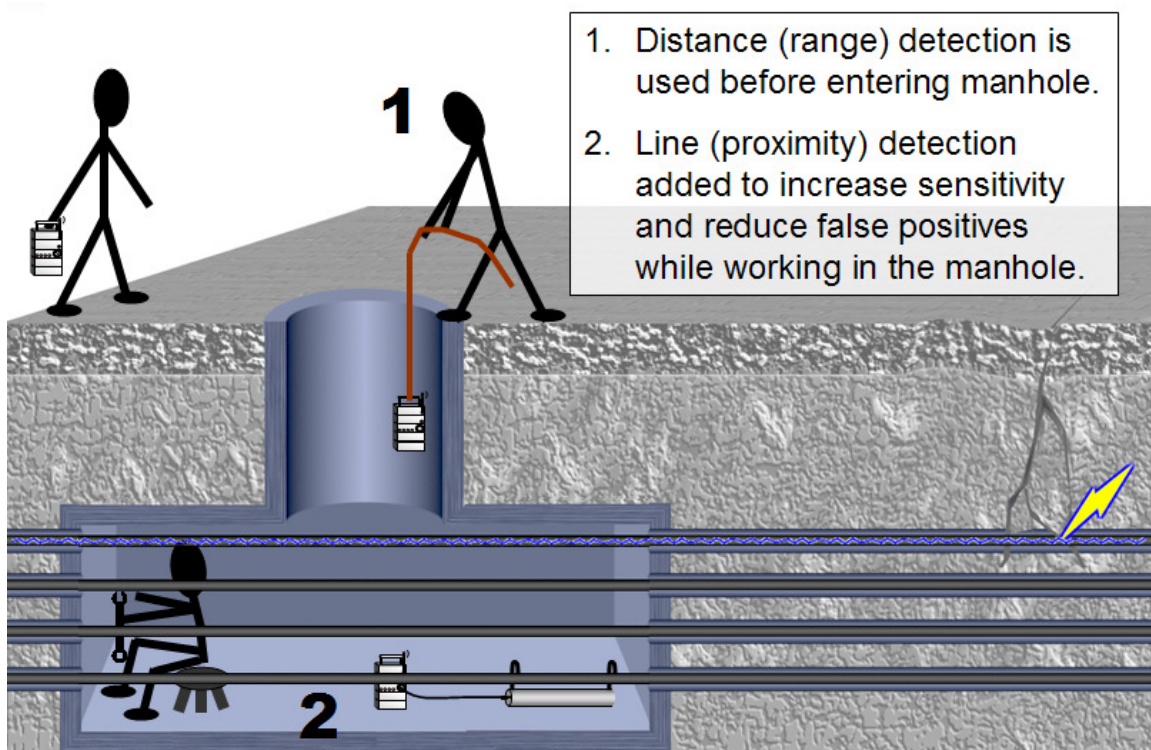


Figure 1. Illustration of Proposed use of Arc Detection System.

Problem Statement

Underground cables that develop weak insulation or poorly insulated connection points can develop into fatal hazards. Cases have been documented involving fatalities due to energized metallic objects and underground fires ignited by electrical arcs. The focus of this

research is on arcing sources that are responsible for manhole fires and explosions. Currently, electric utilities have no type of detection apparatus available, mobile or handheld, for scanning a designated environment for locating arcing faults.

The purpose of this investigation is to demonstrate if an algorithm can positively identify electrical arcs caused by faulty underground cables and develop a device that will give underground utility workers early warning that nearby arcing exists.

CHAPTER 2

LITERATURE REVIEW

Arc detection has been around for several decades. Only recently has it been brought into our homes with Arc Fault Circuit Interrupters (AFCI); however, there is not any documentation on how the two major breaker manufacturers are performing this detection. Even if documented, not all arcing will be captured by an AFCI breaker, and some sources that look like arcing can trip an AFCI breaker.

In the late 1970s the navy was experiencing problems with fires in submarines due to electrical arcing in their switchboard panels. The Applied Physics Laboratory (APL) at John Hopkins University conducted extensive research to create a solution that would disconnect the electricity when these events would occur. Their solution did not require detection of mild arcing or an incipient fault. Instead, they required a quick action of opening a breaker just as the large current fault occurred. Their main objective was to protect the hull of the submarine from being compromised and reduce chances of fire and nauseous smoke feeling the ship. Although this and other literature reviews do not specifically cover high impedance arcing, the detection methods are still useful. Table 1 outlines a summary of sensing methods and challenges from this literature review.

Table 1

Summary of Detection Methods from Literature Review

Detection Methods	Theory	Results from Literature
Direct Voltage & Current Waveform Measurement (Lee, Trotta, King, 2004, p. 12)	Look for signatures in waveforms signals that could signify arcing.	Was able to detect arcing; however, distinguishing between arc signals and conductive signals from large loads was difficult.
Optical Sensors (Land, Eddins, Klimek, 2004, p. 148)	Look for the physical light generated from the arc flash.	Worked as a fast response for disconnecting electricity before an arc melted through a metal enclosure.
Thermo (Land et al., 2004, p. 143)	Detect change in temperature in various places in the system due to arcing, loose, or fault connections	Required too many wires for thermocouples in order to localize; in addition, they would be destroyed by the arc before making a decision. Thermal imaging was too intermittent, later designed a thermo ionization detector that worked in an enclosure.
Pressure Measurement Inside Enclosures (Land et al., 2004, p. 143)	Detect rise in pressure before onset of damage. Normally the doors would be blown off the enclosure during arcing events.	Very small pressure changes which require expensive sensors. This application was used in a submarine environment where pressure is usually equalized.
Sound Recording (Land et al., 2004, p. 143)	Microphone with 50 kHz response and wide range could detect the sound an arc would produce.	At the time they did not have enough signal processing power to distinguish between arcs and other sounds in real time. In addition, reflection of sound resulted in some cancellation, other work used a Pressure Zone Microphone to reduce reflections.
Detect Smoke and Fumes (Land et al., 2004, p. 148)	Overheated connections would give off smoke and gases from the insulation	In this application, it also responded to paint, diesel generator, and other gas fumes.
RF Signals, electric and magnetic field antenna. (Rogers, LaRue, 1995, p. 523)	Electric and Magnetic field measurements resulted in strong, rapidly changing signal that could be easily detected.	Not enough signal processing power to distinguish between arcs and other electrical loads, plus localization of the arc signal was difficult due to propagation.

Electric utilities all around the world have to deal with high impedance faults that do not activate protection relays. Part of the detection for these types of faults is arc recognition. In conjunction with the Electric Power Research Institute, various utilities and universities have studied these behaviors of arcing by recording voltage and current waveforms so they can analyze key signatures and develop algorithms for arc identification. Listed in Table 2 are electrical parameters and algorithms that have been measured from these waveforms to indicate arcing.

Table 2

Summary of Parameters and Algorithms from Literature Review

Parameters & Algorithms	Theory	Results from Literature
Crest Factor (Kim, Russell 1995, p. 141)	Crest Factor is Peak divided by the Root-Mean-Square of the waveform. Sporadic conduction of arcing can sometimes occur at various points of increase on the waveform, resulting in a high crest factor.	Arcing was identifiable by a high crest factor. However, other loads such as DC rectifiers would give false indications. A modified crest factor help reduce some of the false positives given by normal loads by including a form factor calculation which includes dividing the peak by the average cycle.
Non-Periodic Algorithm (Lee et al., 2004, p. 12)	Subtracting previous cycle from the next can help filter out common loads whose currents can dominate levels found in high impedance arcing current.	Helps reduce continuous process loads, even those with repeatable harmonic signatures. If the circuit carries a large amount of dynamic loads, the result could lead to some false positives.
Spectral Energy Algorithm (Charytoniuk, Lee, Chen, Cultrera, Maffetone, 2000, p. 1758)	Measures the harmonic & non-harmonic spectral energy content at various frequencies (limited up to 10 kHz).	Detects arcing well; however, either dynamic energy threshold or environment characterization has to be conducted to reduce false indications from various types of loads and grid operation events.
3 rd Harmonic Phase Angle (Kim, Russell, Watson, 1990, p. 1314)	High Impedance Fault current increases odd harmonics and the relationship between the phase angle of the 3 rd Harmonic and Fundamental Frequency.	Good for the shouldering (high crest factor) of a waveform. Other loads, such as DC rectifiers, can give false positives.

CHAPTER 3

METHODS

Before deciding on a particular sensor or algorithm for this application, a survey of the environment was conducted to gain an understanding of what kind of system could be used.

Electrical Distribution Manhole Environment

As illustrated in Figure 2, many electrical distribution systems in major cities are placed underground. To service transformers, junctions, and other distribution equipment the utilities require manhole vaults to gain access. Depending on the density of the city you will typically see a vault from every 100 to 300 feet. Between vaults there are several conduit pipes that carry numerous conductors. When these conductors enter the vault, they are routed through a rack on the side of the wall. Here, splices are commonly made so electricity can be fed in different directions and the power can be distributed throughout the city to form one big mesh network of electrical power.

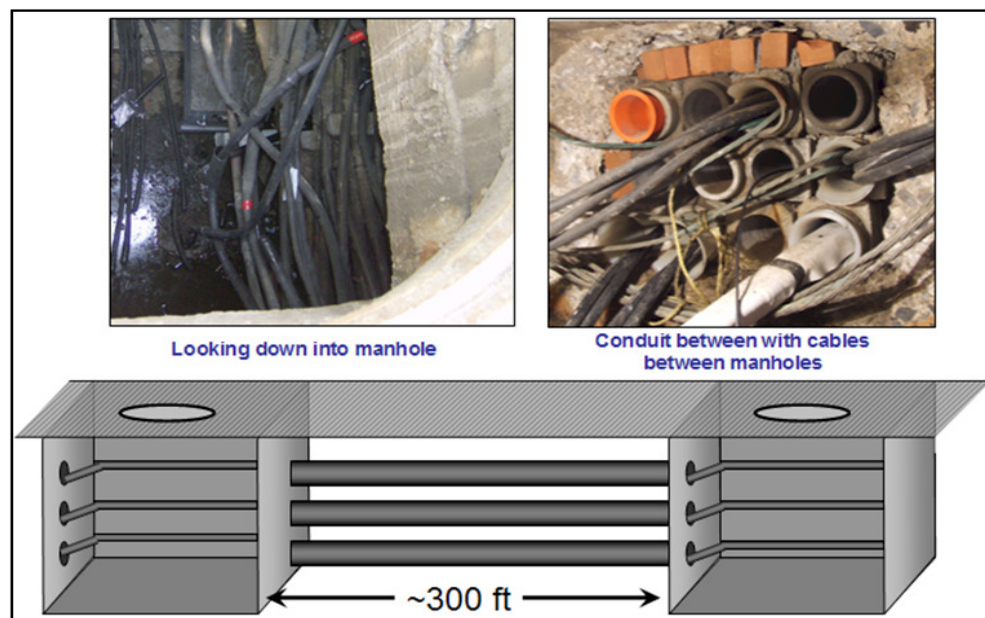


Figure 2. Typical Electrical Distribution Manhole Environment

Sensor Selection

Before collecting data it was necessary to establish what kind of sensor was going to be used to detect arcing in the manhole. Many of the techniques used in the literature research may or may not be effective in a manhole environment.

Optical Sensors

Optical sensing would not be able to look at every part of the system, especially up in the conduit between the manhole vaults. In addition, optical sensing would require a large arc in order to differentiate or contrast the ambient light while working in a manhole.

Temperature Sensors

Temperature sensors such as thermocouples would have to be routed to each conductor in the vault, which can be as many as 10 to 20 conductors. This would require too many thermocouple wires and add too much time for the workers to make the connections. A thermal camera may work well for splices or the conductors in the vault, but again the conductors in the conduit can not be seen with the camera.

Pressure Sensors

Pressure measurement may work well as a means for quickly disconnecting electricity as soon as a large fault begins; however, at that point it would be too late for the worker to leave the manhole. For small, incipient faults with arcing, the change in pressure in a vault would not be great enough to distinguish between normal atmospheric pressure changes.

Direct Voltage and Current Sensors

Because any given manhole vault can have approximately 10 to 20 conductors, it is not feasible to attach current transformers to each one of these conductors for measurement. In addition, sometimes arcing may occur up stream from the vault, which will not draw current past the current sensor. To collect voltage would require the insulation of the cables to be pierced by a probe. This was undesirable due to compromising the insulation of the cable.

Magnetic Field Sensor

Being just one sensor, this is a good substitute for numerous current transformers. Plus, it is quickly deployable from above ground and doesn't need to make contact with the conductors. Adding all the magnetic fields from each conductor in the vault results in a heavily distorted waveform; however, this distortion is in the low frequency range and will result in odd multiples of the fundamental frequency. In addition, higher arc frequencies and non-fundamental frequencies will still be detectable. One problem that still remains is arcing from upstream will not supply current by the vault for this sensor to detect.

RF Electric Field Sensor

Just as AM radios pick up static from lightning, switches, and motors, they also can detect arcing in a manhole. In addition, it can be detected from any direction and would not require an arc to be downstream as with the magnetic field. This sensor could easily be deployed as well from above ground and would not require any contact with the conductors. The main concern is whether an arc signal can propagate through the conduit from over 300 feet away and give a large enough signal to discern arcing. Another concern is the very loads mentioned above can give a false positive indications of arcing. Neon signs are another load that gives false

indications. They are one of many types of loads that use switching power supplies that emit high frequencies. In an environment like New York City there are numerous lit signs with power supplies. Also, static electricity from humans walking can create high frequency signals that can interfere with signals for interpretation.

Sensor Development

Due to each sensor having different fallbacks, it was best to combine at least two different methods for sensing an arc. Both the magnetic and electric field sensors compliment each other in their use. Both can easily be deployed above ground and do not require contact with the conductors. The magnetic field is more efficient in collecting the lower frequency bands, while the electric field would collect the high frequency spectrum. Where the magnetic field will not be able to detect arcing up stream, the electric field can. Where the electric field is susceptible to noise, the magnetic is only susceptible to what's being conducted.

Magnetic Field Sensor

Magnetic antennas are commercially available and commonly come in two forms, loop or ferrite rod. As shown in Figure 3, the loop antenna is larger than the ferrite rod. Both antennas can be designed to measure frequencies as low as 20 Hz and as high as 60 MHz. The loop designed is used more as a directional antenna, while the ferrite rod antenna is designed for more sensitivity. Due to the sensitivity and smaller size, the rod antenna was chose for this project.

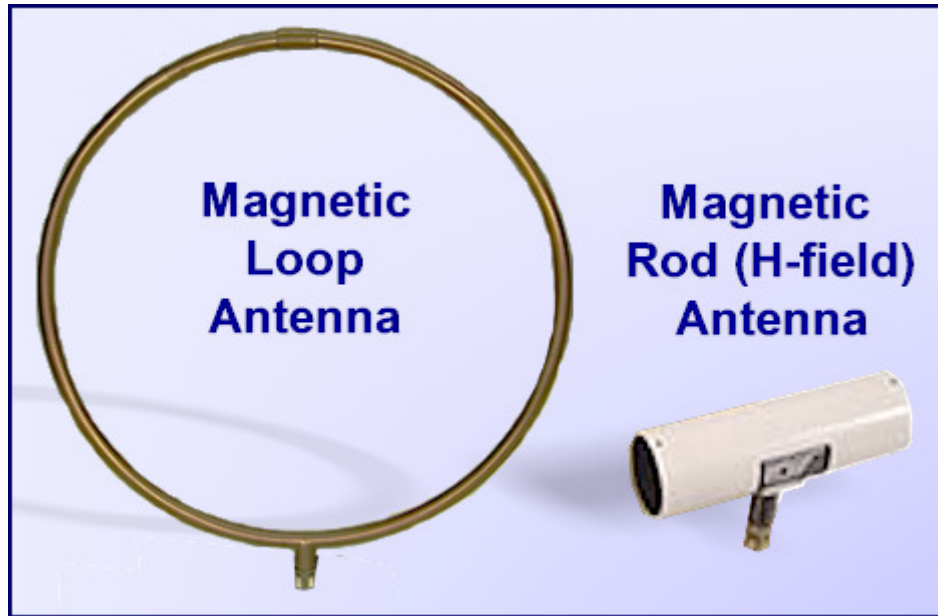


Figure 3. Common Magnetic Field Antennas

The sensitivity of the magnetic field antenna depends on its orientation to the conductor. The maximum field is measured when the antenna is perpendicular to the conductor, allowing the magnetic flux to flow through the ferrite core. In a manhole multiple conductors can be spread along all four walls from top to bottom of the vault. For this reason it was necessary to put together multiple antennas to form one additive multi-axis antenna that would be able to sense each of the conductors.

Electric Field Sensor

The first consideration for an electric field arc detection device was a standard AM radio. It is a common occurrence to hear unwanted noise in addition to your normal listening program on an AM radio. This noise can come from various sources near the radio, such as the sound of your automobile engine, lightning storms in the area, or someone operating a blender nearby. All of these sources are similar in that they generate some form of arcing. So naturally we can

theorize that an AM radio will receive the noise created from arcing on a power distribution system.

As shown in Figure 4 below, an amplitude modulated radio works by tuning in a carrier-frequency signal from a radio station somewhere between 520 and 1,710 kHz. This signal is modulated by the audio content that is broadcast from the station. To hear the audio content the radio demodulates the high frequency content from the signal. What remains is the original audio signal produced at the radio station. Arcing contains a wide spectrum of energy, including high frequencies that are within the AM radio band. The radio treats that frequency as a radio-station carrier-frequency and demodulates the signal. What remains is an audible signal that mimics the amplitude fluctuation of the high frequency arcing.

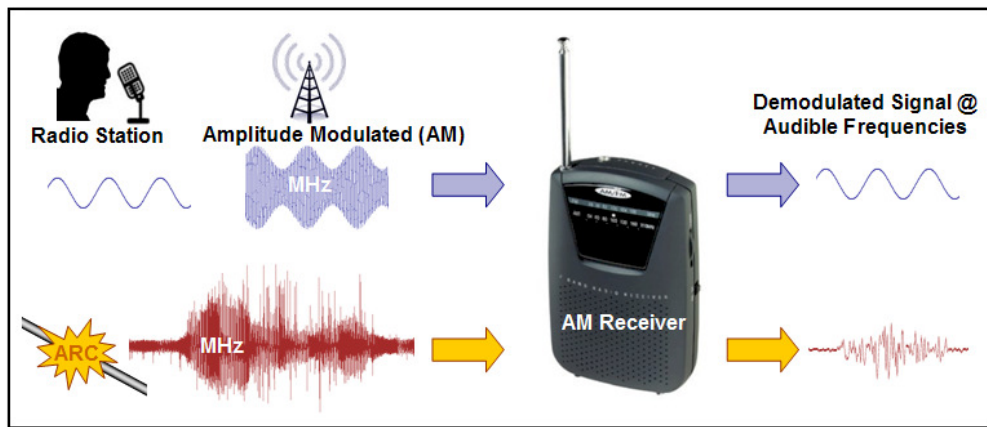


Figure 4. Illustration of How an AM Radio Detects Arcing

There was concern about how the signal would propagate from an arc occurring 300 feet away down the conduit. The maximum reception of 1700 kHz may not be a high enough frequency. The theory was that the conduit may act as a waveguide; however, the conduit is typically 8 inches in diameter. If we compare this to a common rectangular waveguide that has a broad side of 8 inches, we would get an estimate cutoff frequency for 800 MHz.

Another theory is the conductor would act as an antenna, reflecting the high frequency electric field of the arc. As shown in Equation 1, if we use a wavelength equation for a 30 meter length of conductor antenna, the average length from manhole vault to vault, we can calculate a target frequency that a radio might need to receive.

$$f = \frac{v}{\lambda} = \frac{3 \times 10^8 \text{ m/s}}{30 \text{ m}} = 10 \text{ MHz}$$

(1)

Where

v is velocity, which we use the speed of light,

λ is the wavelength

f is the full wavelength frequency

To support this theory and target a radio frequency, a test was conducted in a field environment. For this test setup, as shown in Figure 5, a custom made arc source constructed of carbon rods was inserted into a conduit 300 feet from our sensors.

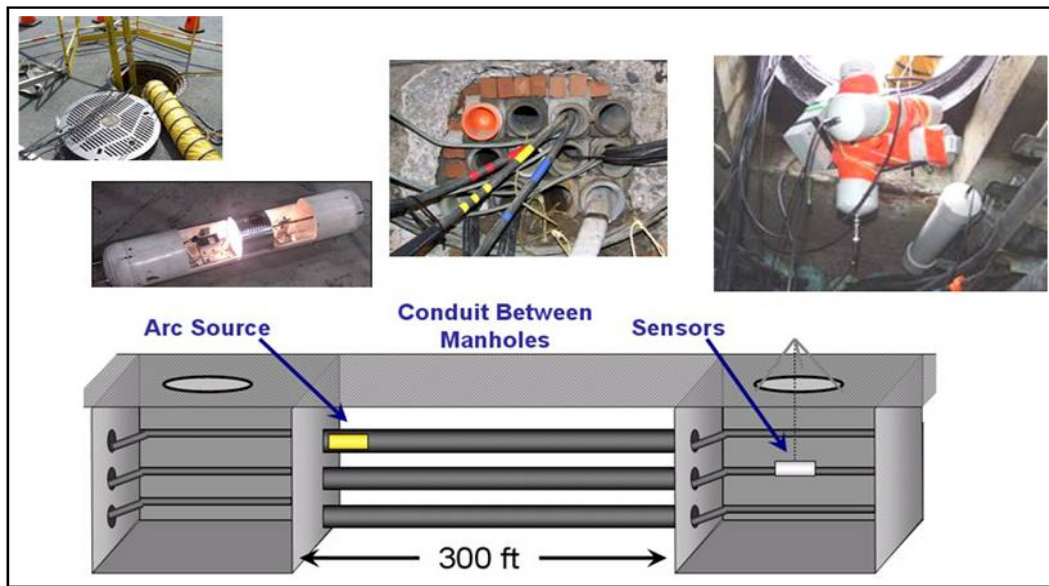


Figure 5. Illustration of Field Test Setup to Measure Radio Frequencies in a Manhole

In addition to our AM radio, an e-field measurement was taken using a commercial manufactured RFI Locator made by Radar Engineers. The receiver could be tuned from 500 kHz to 1000 MHz, well within our theoretical range of 10 MHz. As the arc was being generated in 5 second on-off intervals, the receiver was being tuned for maximum reception of the arcing signal. As can be seen in Figure 6, the receiver could detect when the arc was generated. Based on the signal strength, it was found that the maximum amplitude was received between 2.5 and 5 MHz. Our AM radio could not distinguish on and off activation of the arc. When close to an arc, the audio was easily distinguishable; however, there was always a substantial amount of background noise that limited the distance from the arc source. Most of the noise was contributed to the automatic gain control of an AM radio. When the radio receives a low signal it will adjust the amplitude gain to compensate, which amplifies the noise floor as well.

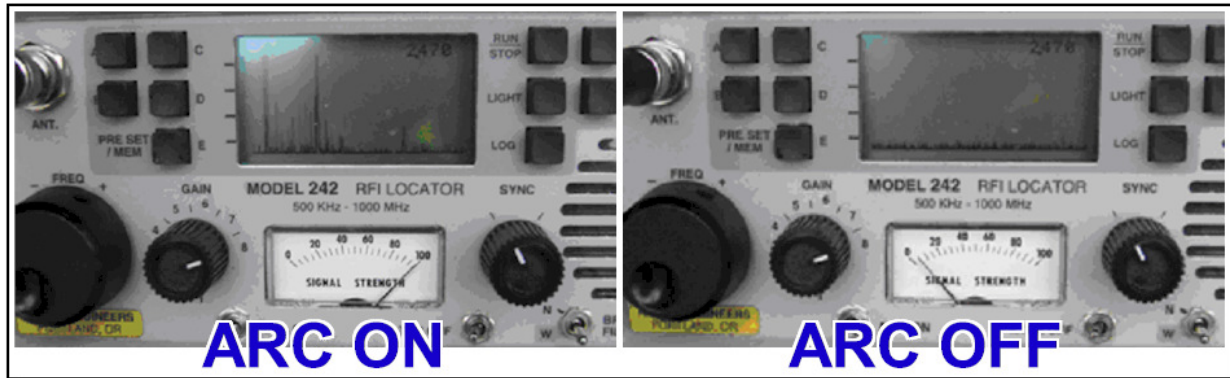


Figure 6. RFI Locator Indicating when Arcing is Present

For our e-field detection unit we selected a hand-held RFI receiver, shown in Figure 7, that was also manufactured by Radar Engineers. This receiver has the capability to switch between low and high frequency. The frequency ranges were not published with the meter; however, lab measurements show that this receiver is within our range of interest. In addition, this receiver has an audio output that can be output to a digital signal processor for further analysis.



Figure 7. Selected E-Field Detection Unit for Arc Detection System

Arcing Analysis

The sensors alone can detect the arcing signal; however, there are many other signals that can be mistaken for arcing. In order to determine true arcing, an analysis of the key signatures had to be studied. This started with the characteristics gathered from the literature review and observing new signatures from our testing.

Data Acquisition for Analysis

The previous studies captured recordings at slow sampling rates of 3.8 kHz . In addition, the precision was 12 or 16 bit resolution. For this study new recordings of arcing were taken with a Dewetron data acquisition recorder, shown in Figure 8, that could sample up to 100 kHz and 24 bits resolution. The faster and higher precision will reveal higher frequency content and new signatures. Faster sampling could have been taken with a scope; however, the digital signal processor for the final system design was being targeted around 100 kHz sampling rate. Other frequency characterizations were collected with spectrum analyzers. A Hewlett Packard 8594E was used for high frequency measurements up to 2.9 GHz, and a Scientific Research SRS-780 was used for low frequency analysis from 0 to 100 kHz. This characterization was challenging in respect to differentiating from loads or sources of noise that could give false indications for arcing.

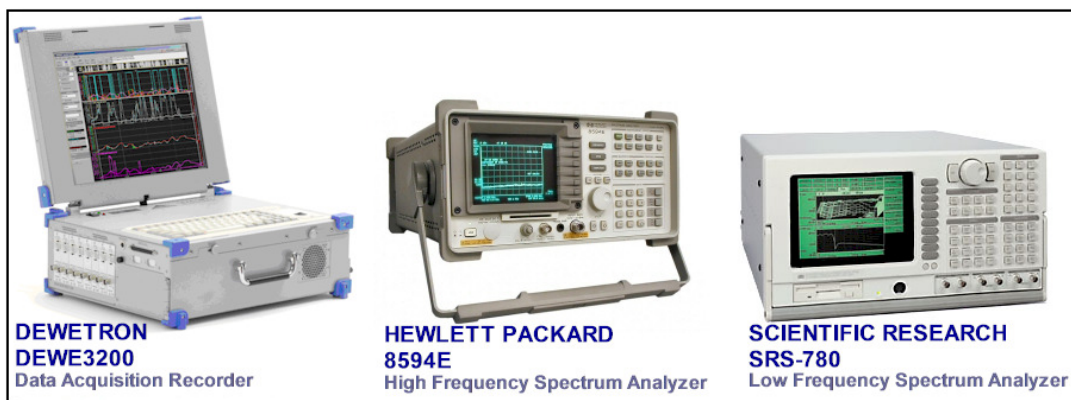


Figure 8. Instrumentation used for Arc Characterization

Arc Characterization

An arc is created when the voltage potential between two objects is high enough that the air between the objects begins to conduct current. This is due to the dielectric strength of air between the two objects. For air a typical breakdown is around 3,000 volts per millimeter. For 170 volts peak, which is peak of a 120 volt RMS waveform, this gap can be in micrometers.

To observe the signatures of an arcing on a 120-volt alternating current (AC) waveform, a test setup was constructed using two carbon rods to draw an arc. As shown in Figure 9, the rods were connected to a line and neutral conductor and placed in series with resistance in order to control potential large inrushes of current. Fine adjustments to the air gap was controlled by a knob connected to a geared linear track through an insulated rod.

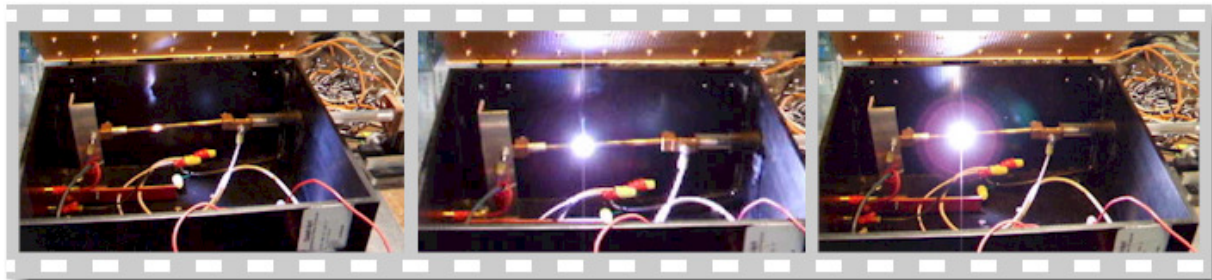


Figure 9. Carbon Rod Arc Generator

Carbon Rod Arcing Waveform Analysis

Figure 10 is a snapshot of a typical waveform while creating an arc across an air gap with carbon rods. Also included is the audio output from our e-field meter to show high frequency content from the arcing. Waveform analysis shows as the voltage starts at zero-cross and begins to increase, the voltage reaches an amplitude [A] that exceeds the dielectric strength of the air gap, this is indicated by the initial arcing [B] created with a few sputtering sparks of low

magnitude current. This generated a region of high frequency content as the air begin to ionize and the dielectric strength of air was being broke down further. As the voltage continued to increase on the periodic half-cycle, so did the current. At this point the conduction is established [C] and less high frequency content is observed. The voltage reaches its peak and then begins to decrease in amplitude. On the down slope of the sinusoid the arc reaches a point when it can no longer sustain conduction [D]. At this point there is not as much high frequency content as the arc dissipates. This process can continue for each positive and negative half-cycle as long as the air gap exists. The shape of this waveform is referred to as shouldering.

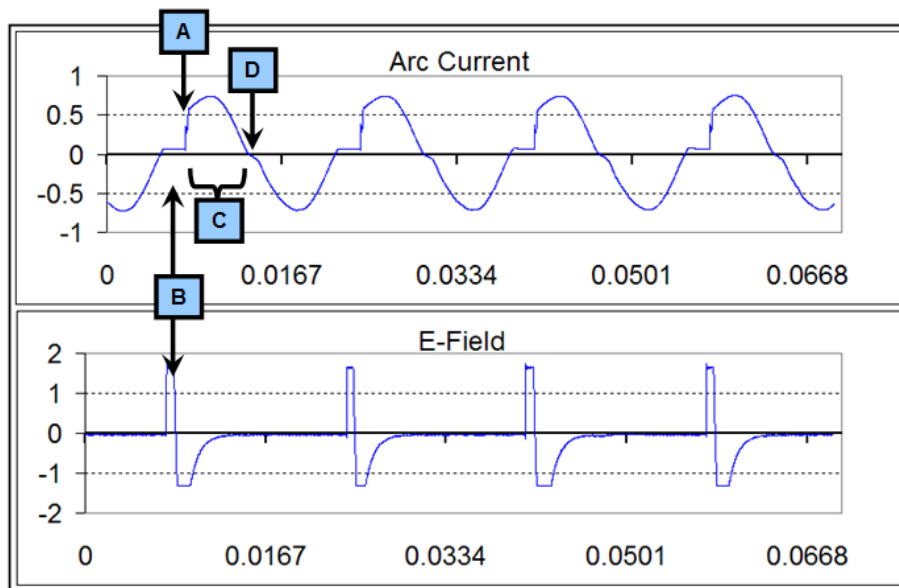


Figure 10. Typical Current and E-Field Meter Output from Carbon Rod Arc Generator

The next waveform, shown in Figure 11, is from the same carbon rod; however, the air gap is shorten to where the tips are practically touching. The same shouldering characteristic is observed, but due to the reduced air gap the arc conducts at a lower voltage amplitude on the waveform. In addition, notice that the high frequency content is almost continuous. This could be attributed to the carbon being close enough to make a conduction path and burning off rapidly.

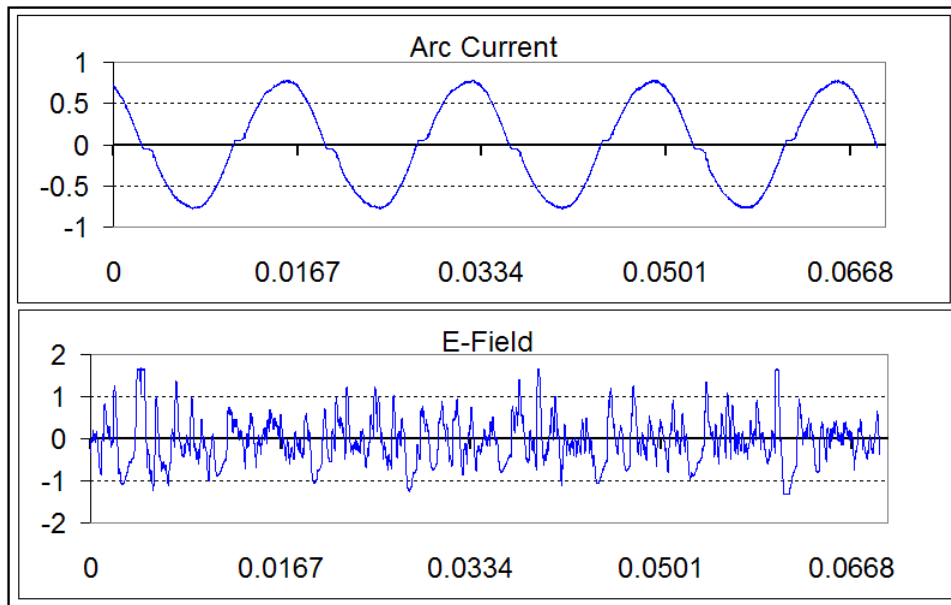


Figure 11. Current and E-Field Output with Minimized Air Gap between Carbon Rods

Crest Factor. At first glance of the waveform we can observe that there is less area under the curve for an arcing current compared to a normal sinusoidal current. A perfect sinusoid will have a root-mean-square (RMS) value that is its peak divided by the square root of two or 1.414 in decimal form. A crest factor calculation is the peak value divided by the RMS value. For a perfect sine wave, as illustrated in Figure 12, the crest factor value is 1.414, the square root of 2. Crest factor values describe the condition and state of the waveform. A value of less than 1.414 indicates a flattening of the wave or low-frequency distortion, and values greater than 1.414 indicate peaking or high-frequency noise. In case of the carbon rod arcing waveform, there is less area under the curve, so the RMS value is lower, which makes the Crest Factor higher. This value can be trended over time and provide a sporadic trend of values for arcing.

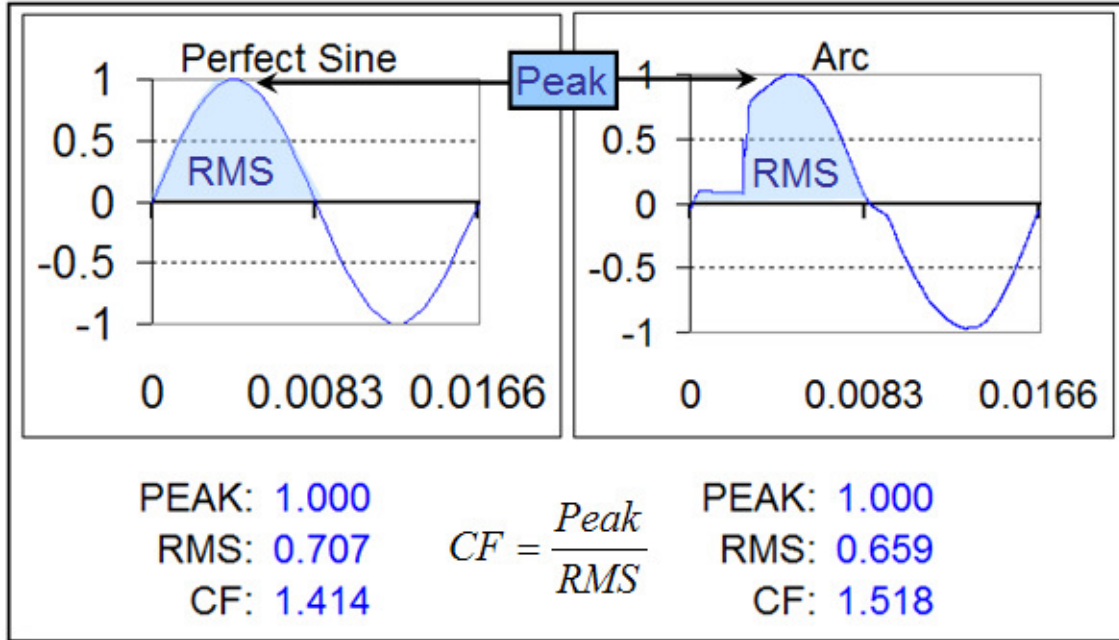


Figure 12. Analysis of a Perfect Sine Wave Versus an Arcing Waveform using Crest Factor

Differentiation. Another observation of the waveform is the rapid change in amplitude as the arc is established. This can be measured by differentiation, which is a method to calculate the rate of change of a dependent value y (*current amplitude*) with respect to the change in the independent value x (*time*). Shown in Figure 13 is the change in amplitude over time. For this calculation, because the change in time is constant, the value of time was ignored. The absolute value of change in amplitude is sufficient in revealing the sudden change amplitude and can be used as a threshold level of detection.

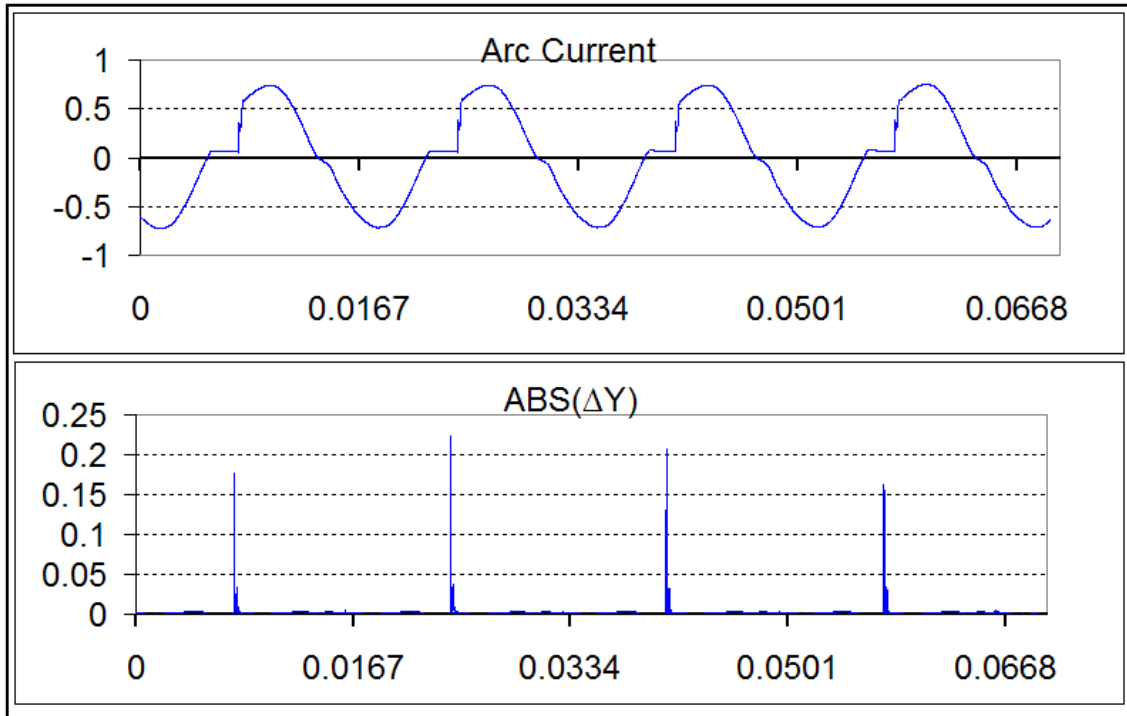


Figure 13. Differentiation of an Arcing Waveform

Carbon Rod Frequency Analysis. Next the frequency components of the waveform were analyzed by performing an Fast Fourier Transform (FFT). Shown in Figure 14 is a 9-second recording with max-min-mean and spectrogram as the carbon rod is conducting an arc. The spectrogram X-axis is frequency in hertz (Hz), Y-axis is time in seconds, and the Z-axis is the amplitude in current, which is illustrated by increased color intensity as seen in the legend. Initially, while the carbon rods are touching between the 0 and 1 second mark, the 60 Hz and odd multiples are dominant. Between 1 and 8 seconds, an arc was generated by creating an air gap between the rods. Here we can see a significant increase in even multiples of 60 Hz as well as the non-multiples, often referred to as interharmonics. Between 8 and 9 seconds the arc grew as the gap was increased further. Again, even more increases in even and interharmonics were observed. The max-min-mean plot illustrates these changes during this period, and highlights

that there is more change in even and interharmonic frequencies than the changes in the fundamental 60 Hz and odd multiples.

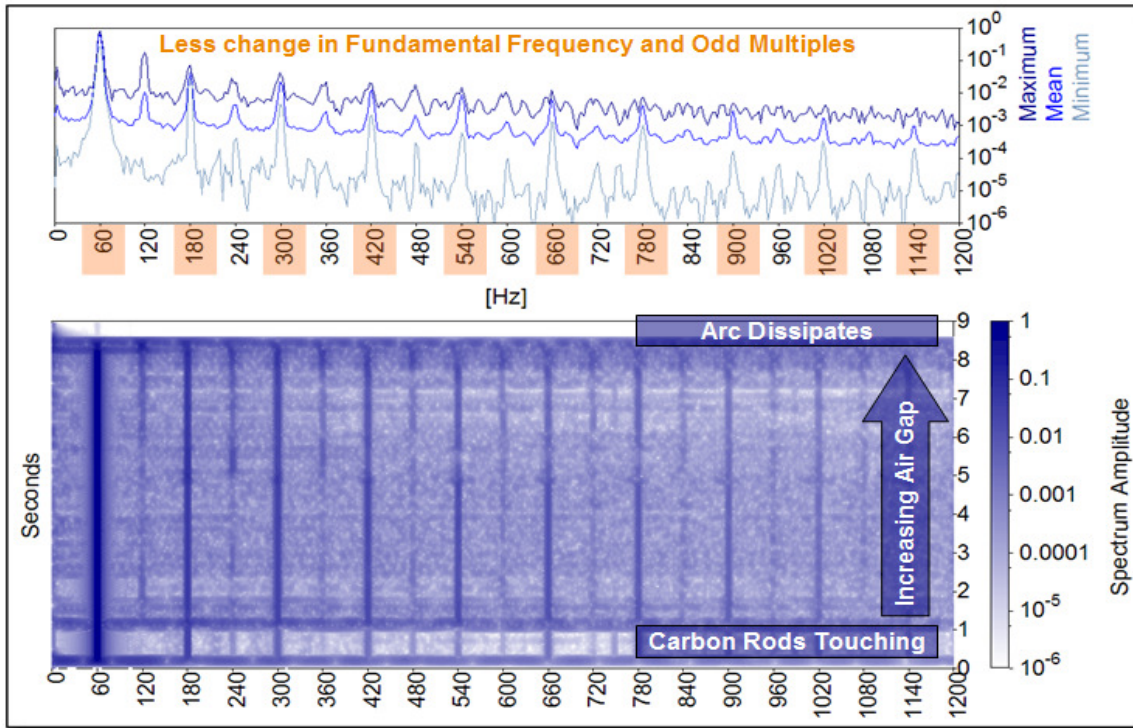


Figure 14. Frequency Analysis of Carbon Rod Arcing

In Figure 15, with a high frequency spectrum analyzer we can see the same increase with arcing in frequencies as high as 500 MHz.

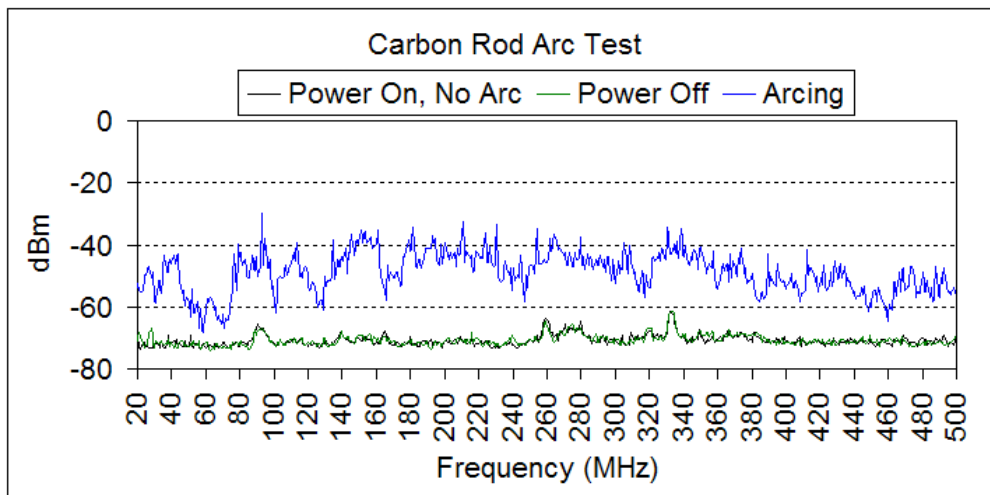


Figure 15. High Frequency Analysis of Carbon Rod Arcing

Sand Slurry Arc Source

The carbon rod arcing seemed to be rather continuous and generally a large amount of arcing once generated. To give more realistic high-impedance arc that could be achieved in the field, a second setup was constructed to mimic a line making contact with soil. The arcing source, shown in Figure 16, is a sand slurry mixture with the neutral conductor buried in the sand while the line conductor is drawn across the top of the mixture. This setup also used a series resistance to limit current. With this setup, smaller non-continuous arcs can be generated with higher impedance.



Figure 16. Sand Slurry Arc Generator

Sand Slurry Arcing Waveform Analysis. The sand slurry mixture produced various magnitudes of arcing and various wave-shapes as well. Shown in Figure 17 are just a few of the waveforms produced. This test added more unsymmetrical periodic cycles than the carbon rod arcing. For example, looking at waveform A and D, the positive half-cycles vary greatly compared to the negative half-cycles. Waveforms A and C show the same shouldering effect as was seen on the carbon rod arcing. Sometimes the waveshape was almost a perfect sinusoid, as shown in waveform B. Looking at waveform D we can see significant high frequency noise on the peaks of each half-cycle. This burst of high frequency content occurs at a 120 Hz rate, which can be used to identify arcing from a 60 Hz source. To see more of these various waveforms, see Appendix A.

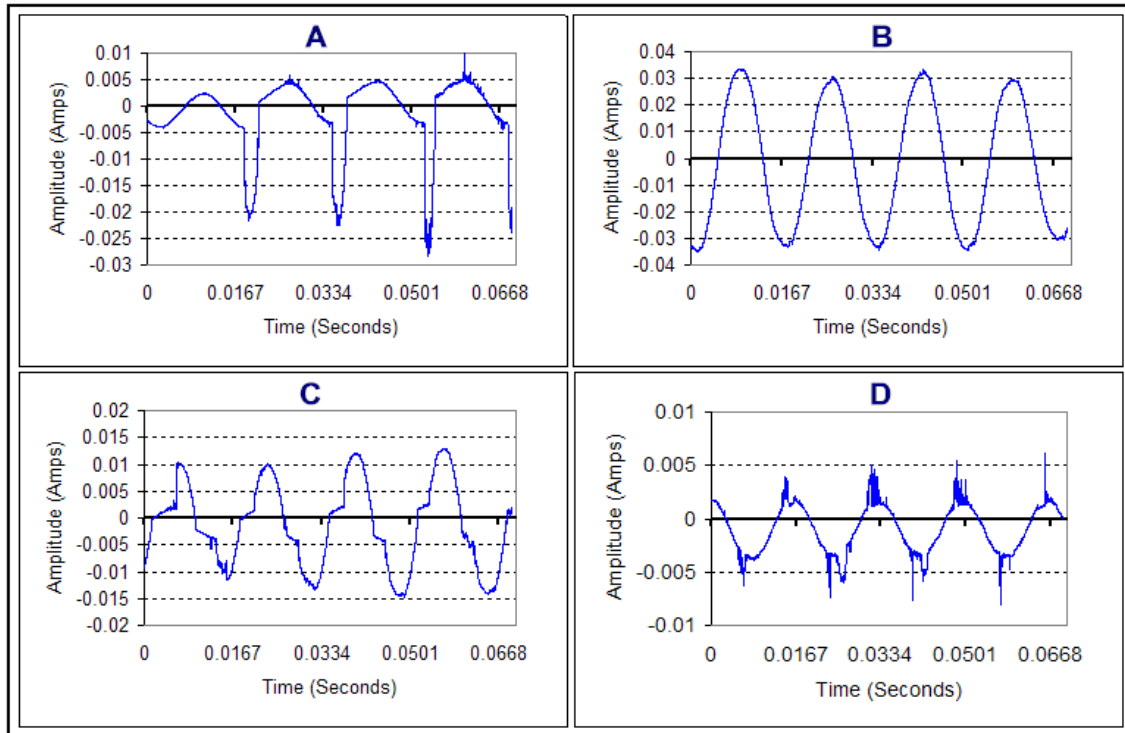


Figure 17. Varying Waveforms Produced from Sand Slurry Arc Generator

Sand Slurry Arcing Frequency Analysis. Looking at a 23-second sand slurry arc, as shown in Figure 18, the FFT shows similar increases in even and interharmonic frequencies as well. One major difference is the sporadic changes throughout the measurement. Just as represented through the different waveshapes, the frequency amplitudes are continually changing. The unsymmetrical waveforms we saw above in Figure 17 signify increased even harmonics. In the spectrogram this can be seen as the amplitude increases at 120 Hz between the 10 to 13 second mark.

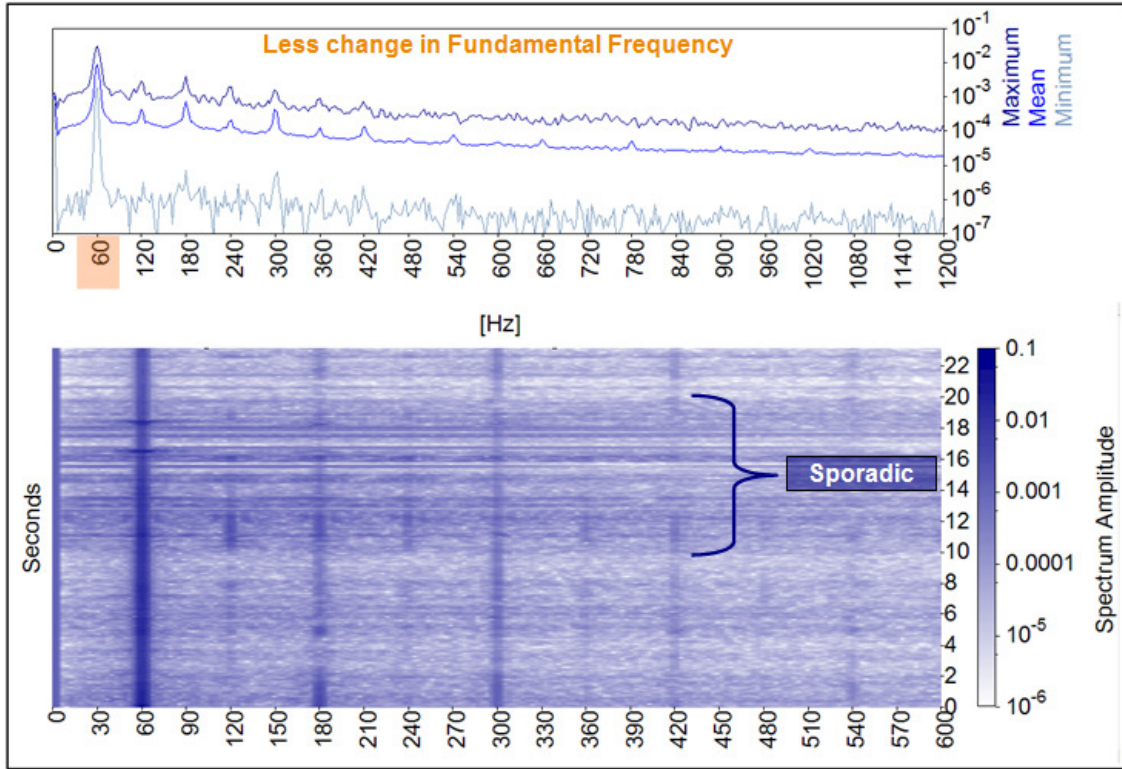


Figure 18. Frequency Analysis of Sand Slurry Arc Generator

Unlike the carbon rod arcing, if other material or elements surround an air gap, such as the sand slurry arc source, less predictable signatures occurred. These elements can be found in a manhole environment.

Manhole Arcing Simulation with Contaminants

The environment above ground can have adverse effects on this underground system. Contaminants such as road salt, grit, sand, and rain water can fill these chambers and conduits, and potentially surround compromised cables. The theory is the contaminants can help establish high impedance conduction paths that can carry an arc. To test this theory a small scale experiment was conducted by taking two insulated cables and compromising the insulation by cutting a small slits down to the copper conductor, as illustrated in Figure 19. The two cables

were placed next to each other in a bed of wet salty asphalt grit and then connected to 120 volts AC. A breaker was added upstream to disconnect the circuit when four amps was exceeded.

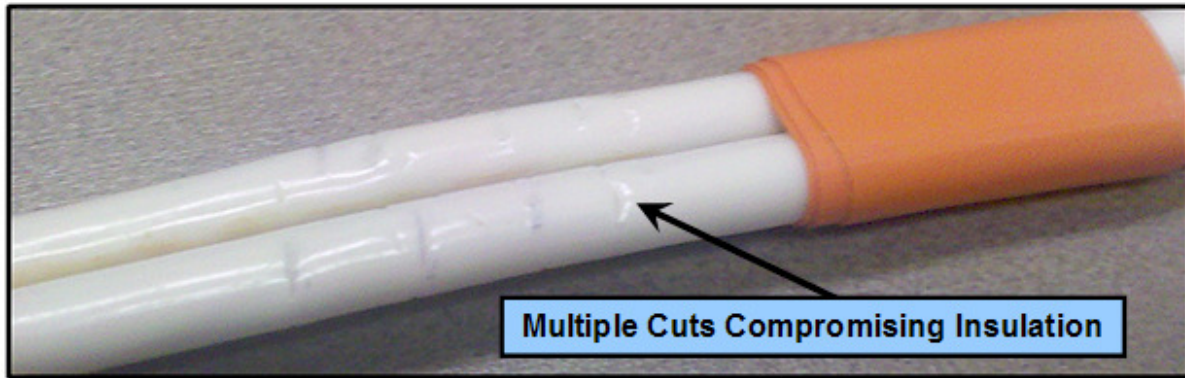


Figure 19. Conductors with Compromised Cuts to Simulate Contamination Process

Initially there was no current being conducted. After 30 minutes, T=00:30, the cables began to smoke and heat up, while the water surrounding the grit began to bubble. A small amount of sinusoidal current, less than 200 milliamps, was being drawn between the line and neutral conductors. At one hour into the experiment the moisture from the water began to evaporate. Small air gaps begin to form causing the first signs of arcing to occur. The arc would last a few milliseconds, extinguish, then more moisture would move in to form a high impedance conduction path. At this point the conduction and arcing was sporadic and drawing up to 750 milliamps. The arcing waveform was heavily distorted, while the high impedance conduction was a sinusoidal 60Hz waveform. At T=01:05 most of the moisture was gone from around the cables and was no longer drawing current. A little more water was added to moisten the soil, but not submerge it. After a brief arc with high frequency current, the circuit began drawing normal sinusoidal current as moisture bubbled around the conductors. At T=01:15 the circuit was arcing the majority of the time, which was drawing up to 1000 milliamps of current. At T=01:18 the insulation was severely deteriorated and creating carbon traces between the line and neutral

conductor. With a large amount of arcing and heavy smoke, the fault current quickly exceeded 4 amps and tripped the breaker up stream.

It is concluded from this test that contamination in the form of road grit, salt, and water aids in creating high impedance conduction paths as well as arcing. The combination of the two was sporadic and unpredictable. The waveforms observed during the testing showed that during the early stages, the high frequency signatures from arcing was not as predominate compared to the high impedance 60 Hz being conducted through the moisture. However, as seen in Figure 20, once the insulation was melted and the water vaporized from the heat, the bare conductors were exposed to the air gaps in the moist grit, which led to increased arcing. The last 5 minutes the arcing was dominant and begin to look more like the arcing produced with the sand slurry test setup.

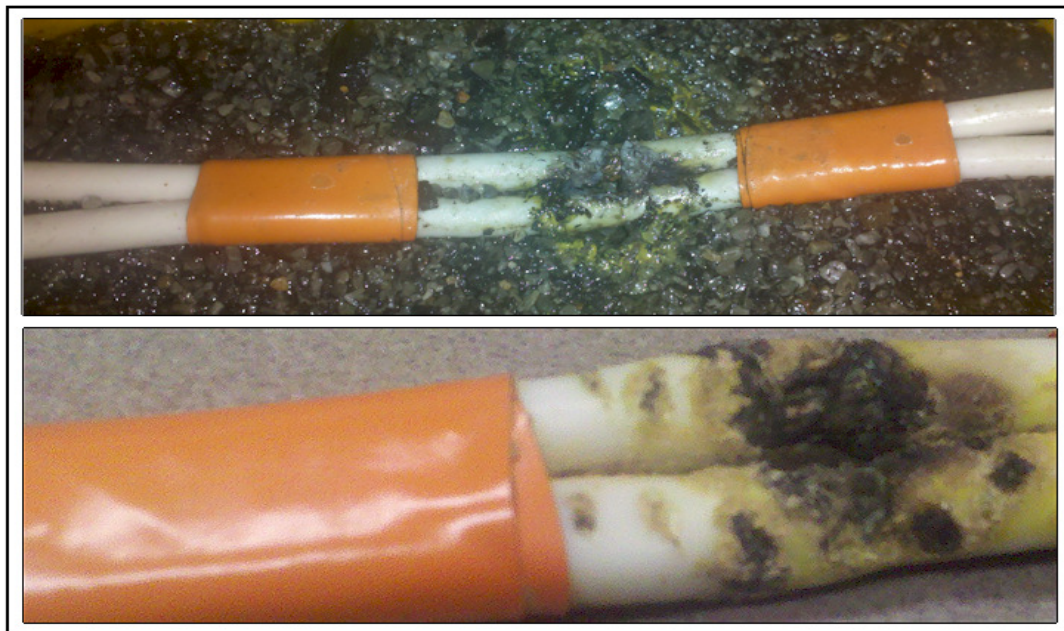


Figure 20. Damage to Conductor Due to Compromised Cuts and Contamination

E-Field Data Analysis

Most of the analysis to this point is using current measurements along with the high frequency indication from the e-field meter. Upon further observation, it was shown that the output of the E-field meter might be providing a demodulated signature that could be analyzed in much the same way as the current / H-Field data. The theory is the high frequency amplitude is being demodulated to the audio output much like an AM radio would demodulate a signal. Figure 21 shows a current waveform and e-field meter output for the sand slurry arc source. With the high frequency content being detected on every peak, the amplitude modulation would be two times the fundamental frequency, which would be 120 Hz.

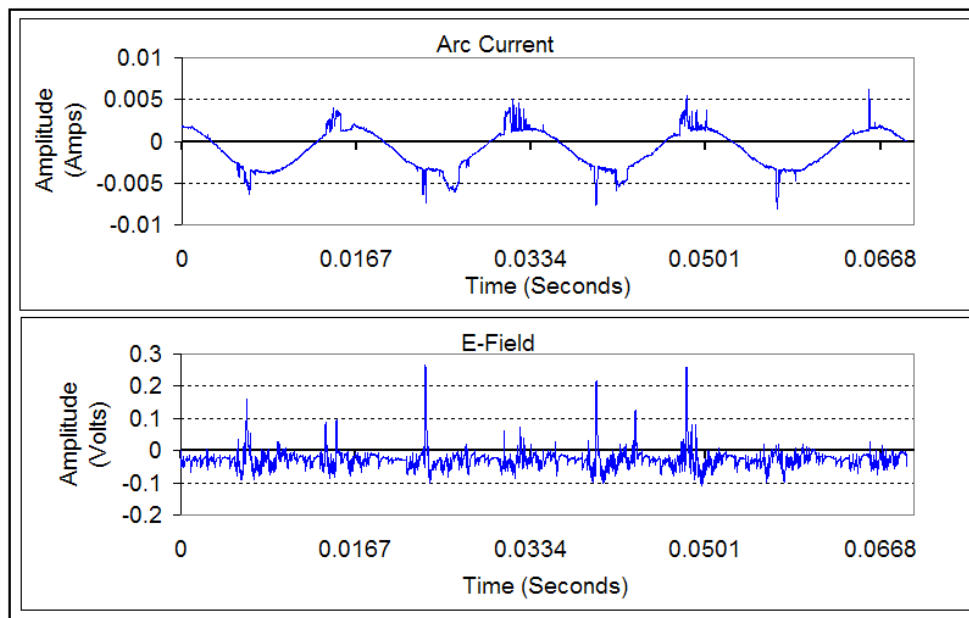


Figure 21. Current Waveform and E-Field Output from Sand Slurry Arcing

To test this theory an FFT was performed on the same data set. Figure 22 shows that indeed 120 Hz is the dominant frequency for this recording. Three other frequencies are also present, 60, 180, and 240 Hz.

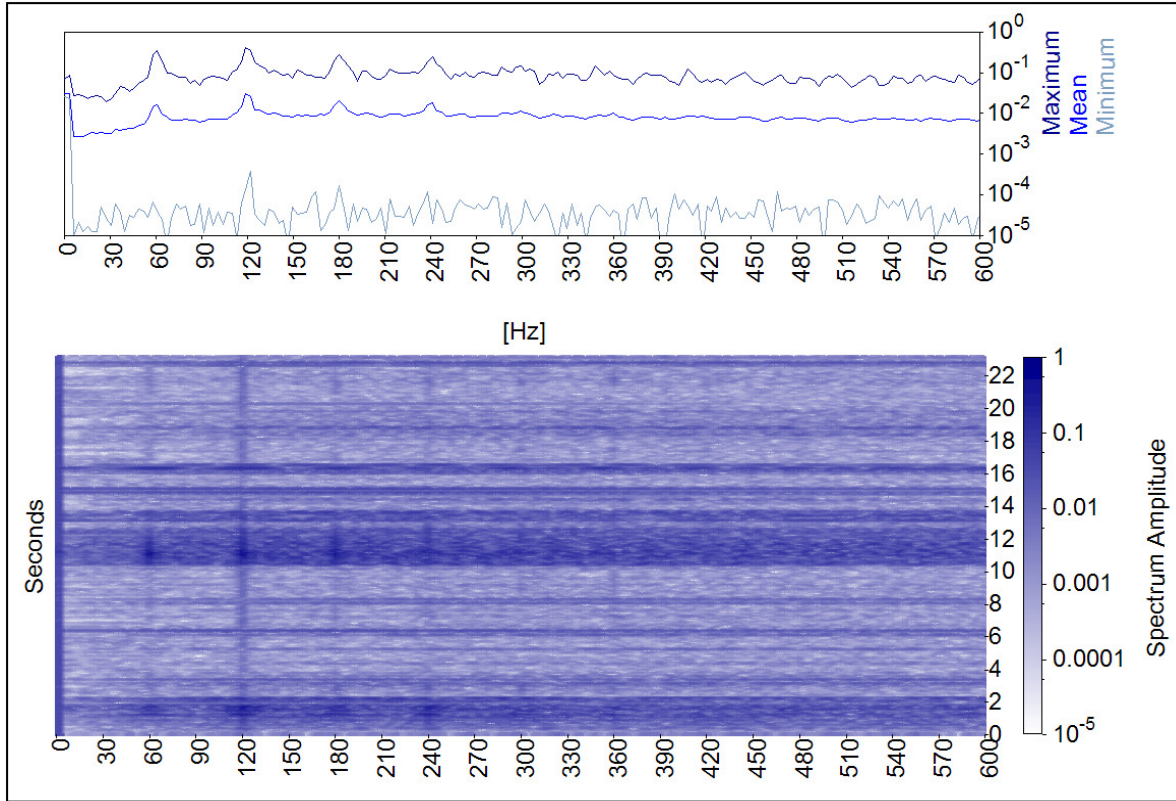


Figure 22. Frequency Analysis of E-Field Meter Output during Sand Slurry Arcing

Another observation is the comparison of the e-field meter output to an AM radio. As shown in Figure 23, the output of the e-field meter is more sporadic, just as we see in the magnetic field data. Again, the smoothness of the AM radio signal can be contributed to automatic gain control that distorts the true demodulated content of the arcing signal. In addition, the output stage of a radio uses low pass filters to help reduce popping and unpleasant sounds that normally a radio listener would not want to hear.

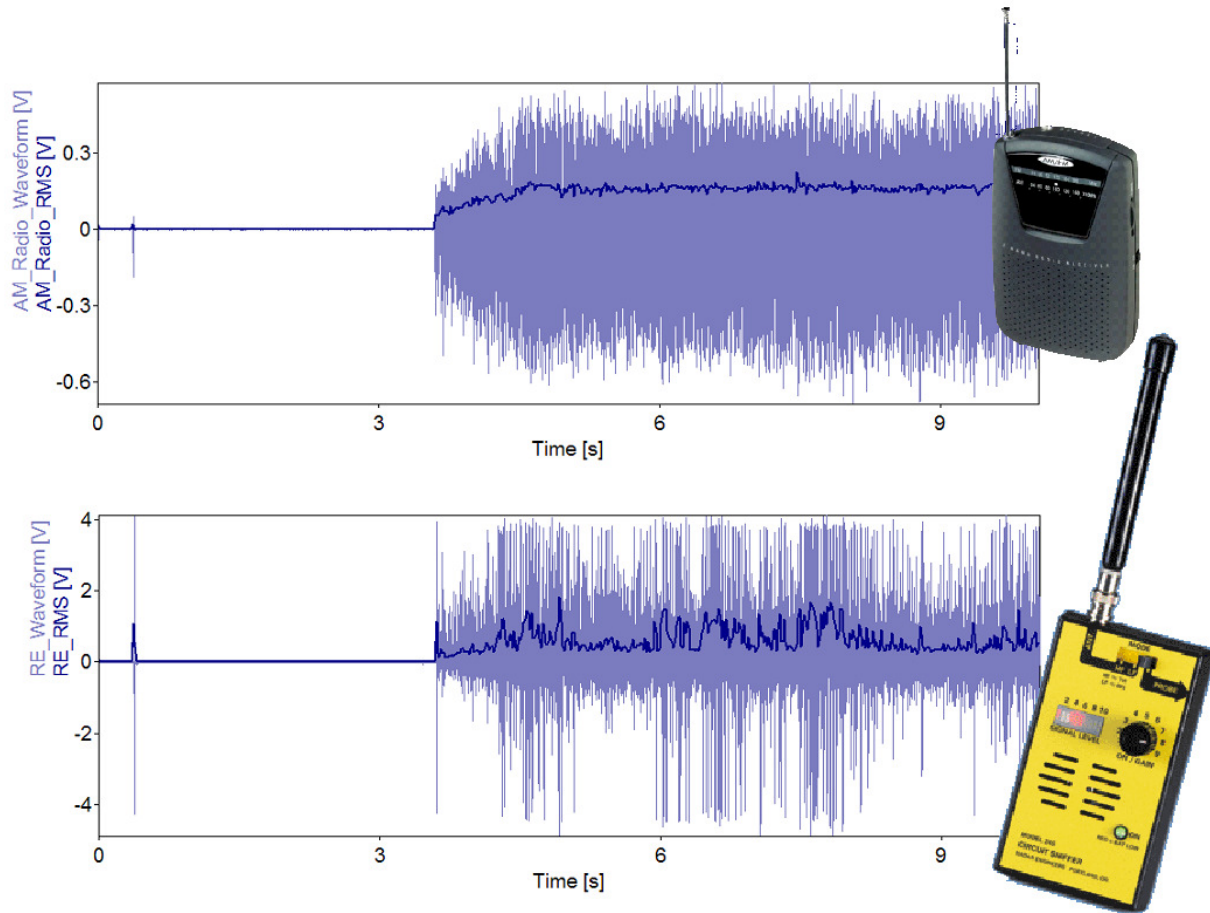


Figure 23. Output Comparison of an AM Radio and E-Field Meter

Potential False Positives

A false positive is a measurement that resembles the characteristics of an arc signature and therefore is reported as an arc, but in reality it is not. For example, one of the characteristics of arcing is the shouldering of the current waveform. As recalled, one of the indicators for shouldering is measuring the crest factor of a half cycle. There are different loads that can give this same signature. Figure 24 illustrates an example showing three different waveforms. One is a silicon controlled rectifier (SCR) for a light dimmer, another is a linear power supply, and the other is from arcing. Each has a crest factor greater than 1.414. However, if we use the

differentiation technique, which locates the sharp rise of high frequency content, we would see that the first waveform on top is from arcing.

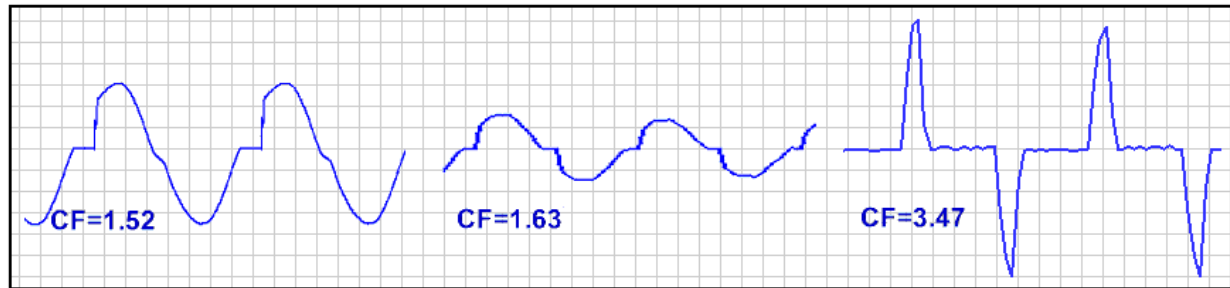


Figure 24. Common Waveforms that Generate High Crest Factor as a False Positive for Arcing

Before depending on the differentiation method, let's look at another example. A neon sign uses a switch-mode power supply (SMPS) that generally operates in the kilohertz (kHz) frequency range. As shown in Figure 25, this high frequency content is appearing at the peaks of the current waveform, much like some of the arcing waveforms. The differentiation analysis yields the same quick changes in current that could be mistaken for an arc. In this case we could use another detection method using the interharmonic or even harmonic measurements because the waveform is symmetrical and rule-out that this waveform is an arc.

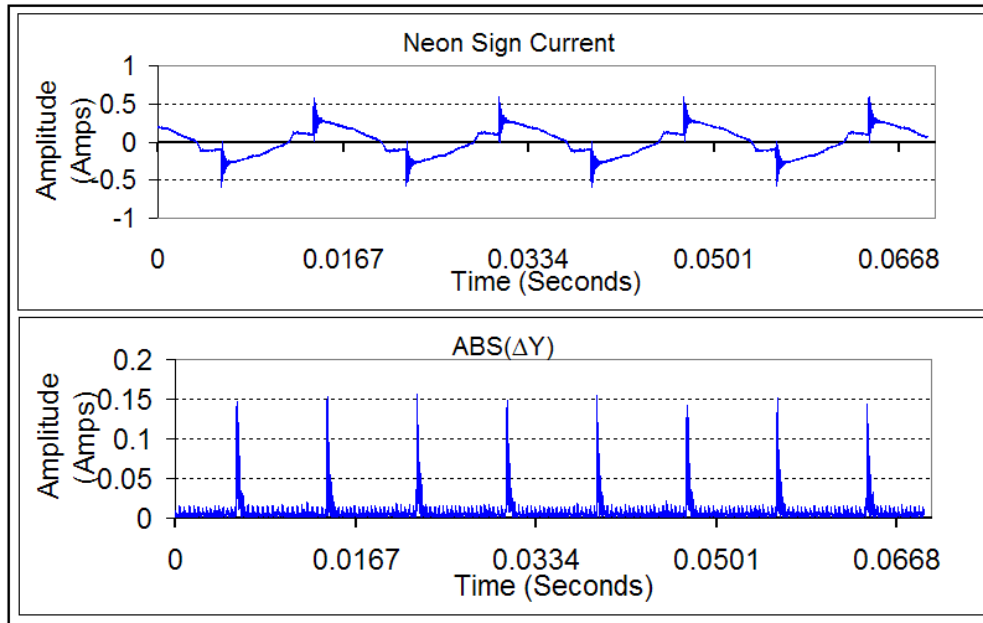


Figure 25. Neon Sign Current and Differentiation False Positive for Arcing

If we depend on the non-multiple harmonic method, we still are faced with other loads that can trigger as a false positive. Cyclo-converters and pulse width modulation (PWM) converters are devices that purposely change the fundamental frequency so their loads do not have to rely on the utility frequency. The slight difference in frequency increase interharmonic amplitudes on the grid. If an industrial facility has numerous loads that are continually switching on and off can produce additive currents that contain some interharmonic or even frequencies. Another common source can come from large loads that temporarily saturate down-stream transformers. The unsymmetrical distorted current is loaded with interharmonics that could be mistaken for arcing in the lower frequency region. However looking at higher frequencies, such as the MHz region with the E-field sensor, we can rule out the possibility of arcing.

Because the E-field sensor samples frequencies in the MHz region, it could prove difficult to find a source that could give a false positive for arcing. However, sometimes arcing itself can be a false positive for arcing. In the case of subways that use a direct current (DC) rails

to power the trains, often referred to as the “third rail”, they can draw significant size arcs when making contact. Another source can come from DC motors that use brushes. These types of motors use brushes to supply current to the rotor coil. These brushes arc as they move from one commutator contact to the next. Figure 26 shows the demodulate output from the e-field sensor while a cordless DC drill is being used nearby. Over time we can see the change in all the frequencies as the drill is being used. If we just look for changes in interharmonics, we can get a trigger for arcing. However, a good feature to observe is that the frequency is practically uniform in amplitude across the spectrum. Recall that the e-field measurement from the arcing source showed higher values for the 60 Hz fundamental, as well as even and odd multiples. With spectrum uniform and showing DC content, both can be used as good indicators that this is not arcing coming from a 60 Hz AC source and therefore can be ignored.

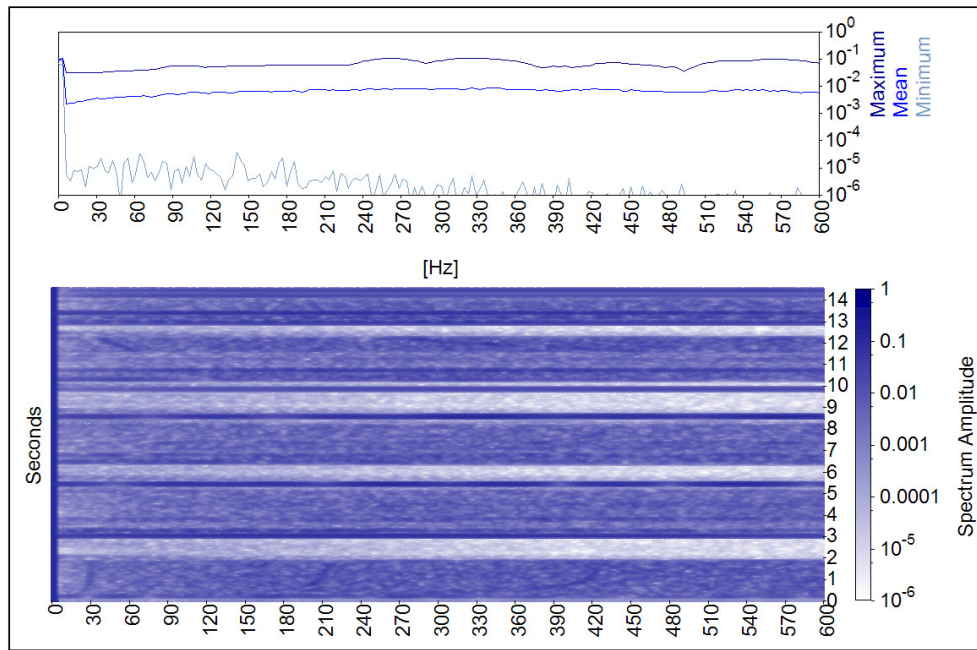


Figure 26. Frequency Analysis of E-Field Output Sensing DC Arcing from a Drill

We can conclude there are many types of loads that give false positives for arcing. More important is no one method is going to be close to a high confidence indicator. Only with multiple detection methods can the high confidence be achieved.

Algorithm Development

When developing an algorithm for arc detection, it was important to use calculations that could be made quickly in order to give a fast early warning response for the worker to exit the manhole. Frequency analysis can consume a lot of processing power as well as take considerable time. In deciding best methods for the sake of response time, only certain frequencies are sampled, and time domain calculations were preferred over frequency calculations. Conversely, being a development prototype unit, we will include as many algorithms as needed for testing purposes. Later models will use less algorithms as further data are collected and improvements are made. With several signatures of arcing established and an understanding of some of the loads that can give false positives, algorithms were constructed for each sensor.

H-Field Algorithm

As shown in Figure 27, the magnetic (H-Field) sensor algorithm contains three root methods for arc detection; percent interharmonics, differentiation, and crest factor. For each method there are three primary stages; threshold level, instantaneous change (Δ), and repetitiveness. As we move down into each stage, it is more likely that arcing is occurring. The threshold-level triggering is simply a static limit. If a certain limit is crossed, the output is triggered. These limits have a high probability of being triggered by false positives. Next, even if the limit is a false positive, a certain level of change is required for the next stage to be

activated. Using a 1st order dV/dT allows steady state data to settle at a zero reference. This acts as a dynamic limit triggering that looks for the dramatic changes. At this level an arc pulse generated from a switch could give a false positive. Therefore, the next stage looks for a number of these dynamic changes within a given period. This trigger responds to the sporadic nature of arcing. For the differentiation method one more stage is added by looking for a 120 Hz repetition rate.

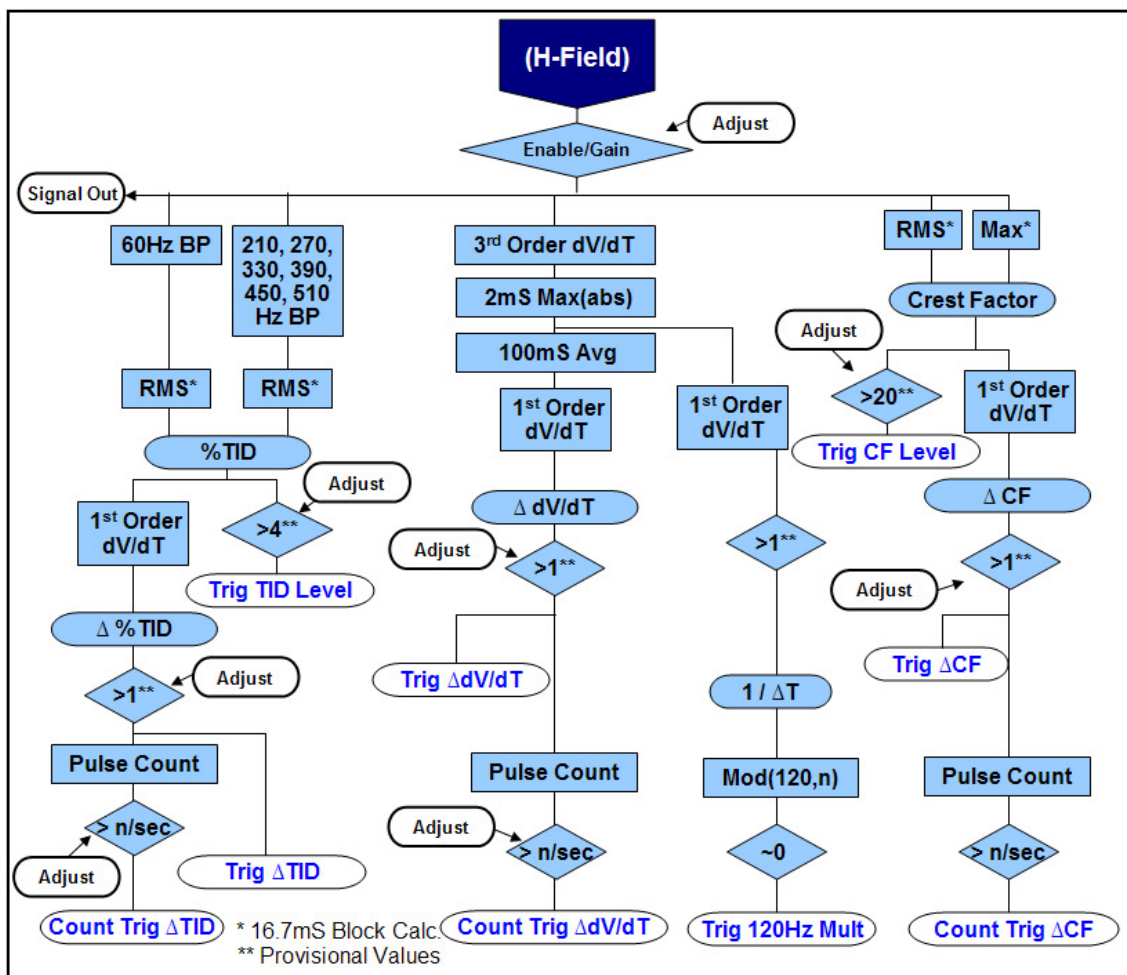


Figure 27. Magnetic Field (H-Field) Algorithm Set

E-Field Algorithm

Figure 28 outlines the algorithms for the electric field. The primary function for this scheme is to determine if the MHz signal is comprised of 60 Hz and whether the signal is sporadic. As already observed, for most white noise and DC arcing the modulated signal is going to be comprised of frequencies with equal amplitude. For 60Hz sources the frequency multiples will be higher than the non-multiples (interharmonics). For this algorithm two multiple frequencies, an even and an odd, are compared to a non-multiple. Depending on the threshold this alarm is triggered. Next, we use the same change method, and repetition as used in the magnetic field algorithm. The first order derivative looks for instantaneous changes, while the repetition counter looks for number of changes in a given period.

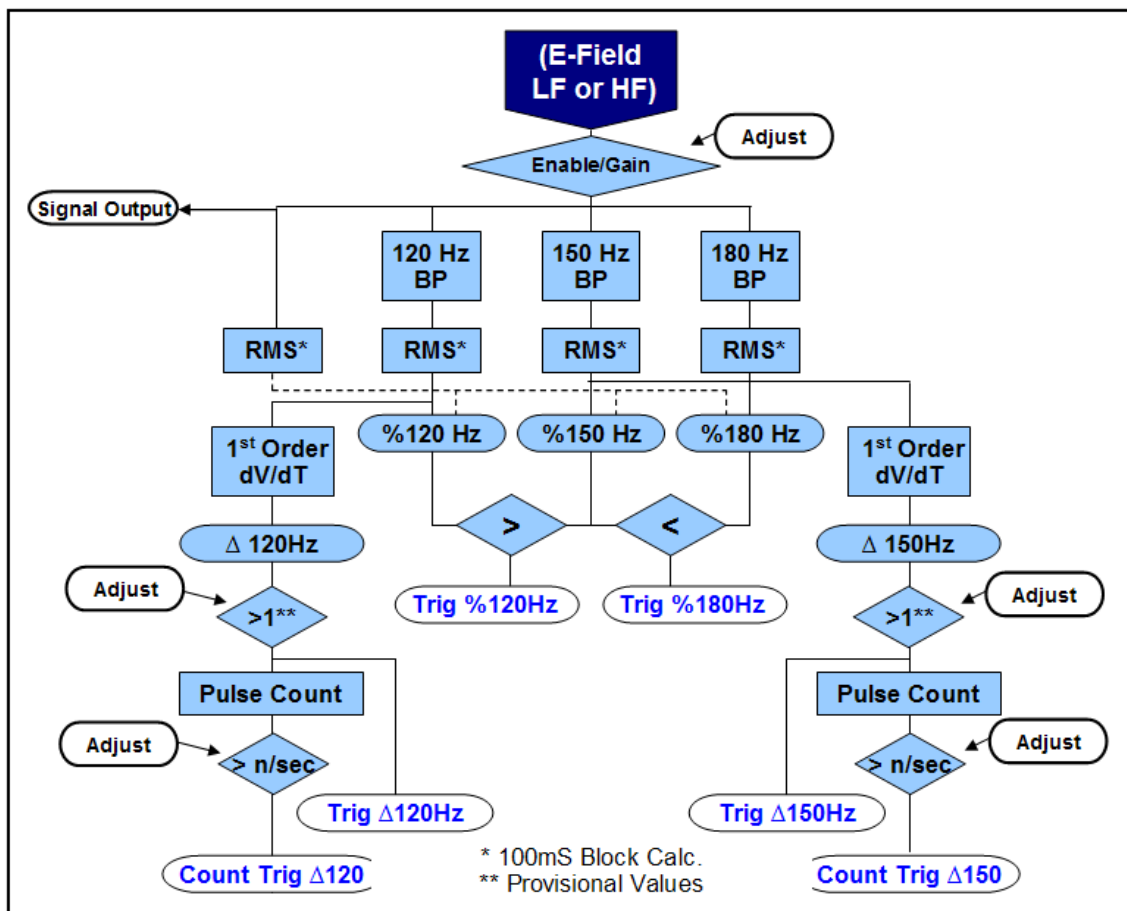


Figure 28. Electric Field (E-Field) Algorithm Set

Alarm Decision Logic

The alarm for each of the algorithms is arranged to give three levels of alarm conditions; low, medium, and high. As shown in Figure 29, the low level alarm will basically sound when either trigger is activated. There is a high probability that a false positive will trigger this alarm; however, being a prototype development unit, this extra sensitivity is being used to indicate possible false positives in lab and field testing. Later, this level may be removed. The medium and high level alarms require the repetitive triggers to be activated. Medium requires any repetitive trigger, while the high level requires all the repetitive triggers.

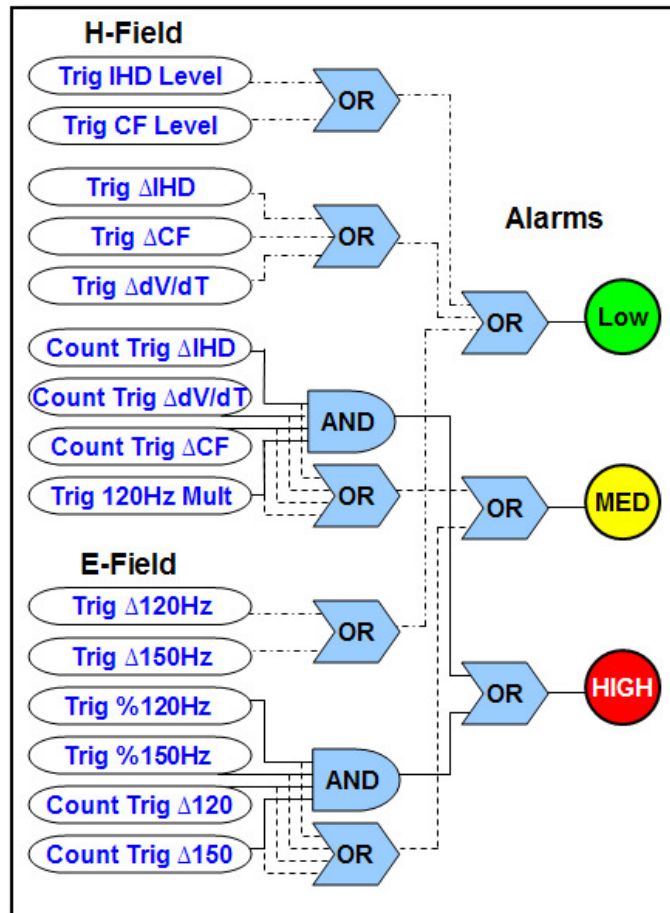


Figure 29. Three Level Alarm Logic Diagram

Digital Signal Processing

With the sensors selected and several arc characteristics and algorithms determined, we were able to move towards selecting a digital signal-processing (DSP) unit. The system selected was a National Instrument's "Compact RIO™" which uses field programmable gate array logic (FPGA) and a co-processor for real-time processing. This unique combination allows for fast processing of the signals within the FPGA and then passes the processed signals to the co-processor for final logic analysis or decision process to set the alarm conditions. The unit comes with numerous signal-conditioning options of which this project used two. One was an analog input card for collecting the sensor data. It has a +/- 10 volt range at 24 bits, and 50kHz sampling rate. The other conditioner was a digital output card used to trigger the lights and speakers as visual and audio alarming. As shown by the screen-shots in Figure 30, the programming was all designed through a LabView software interface that could be compiled and loaded to the Compact RIO™ as a stand alone processing unit.

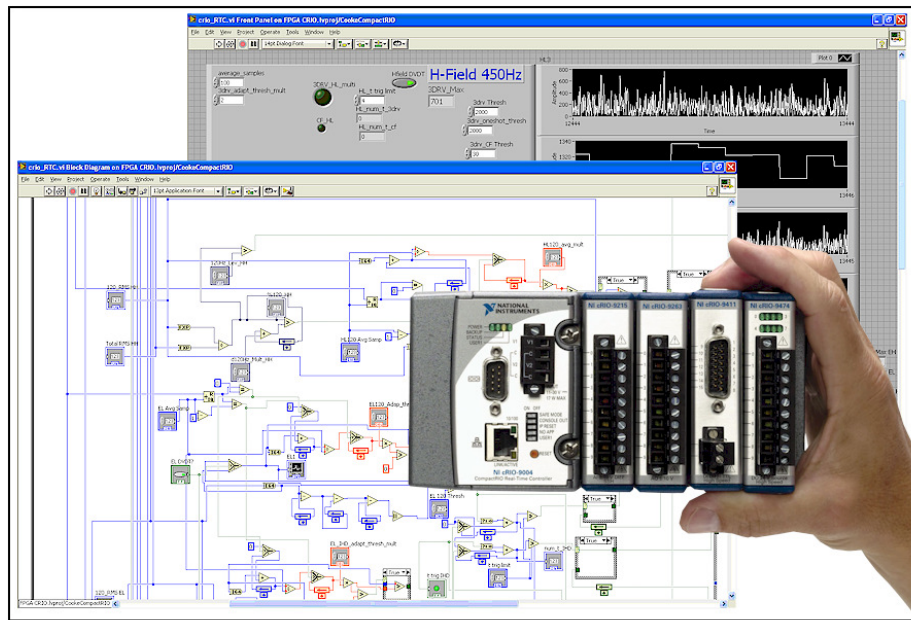


Figure 30. CompactRIO™ Digital Signal Processor with LabView Screen Shots

Design

As shown in Figure 31, a clam shell box was chosen for easy access in case of troubleshooting and flexibility in arranging the design. The electrical field meters and amplifiers for the magnetic field sensors were placed in their own shield cases for isolation and mounted on the top of the chassis plate along with the alarms and light indicators. The Compact RIO™ is mounted in the bottom with the battery pack and charger.

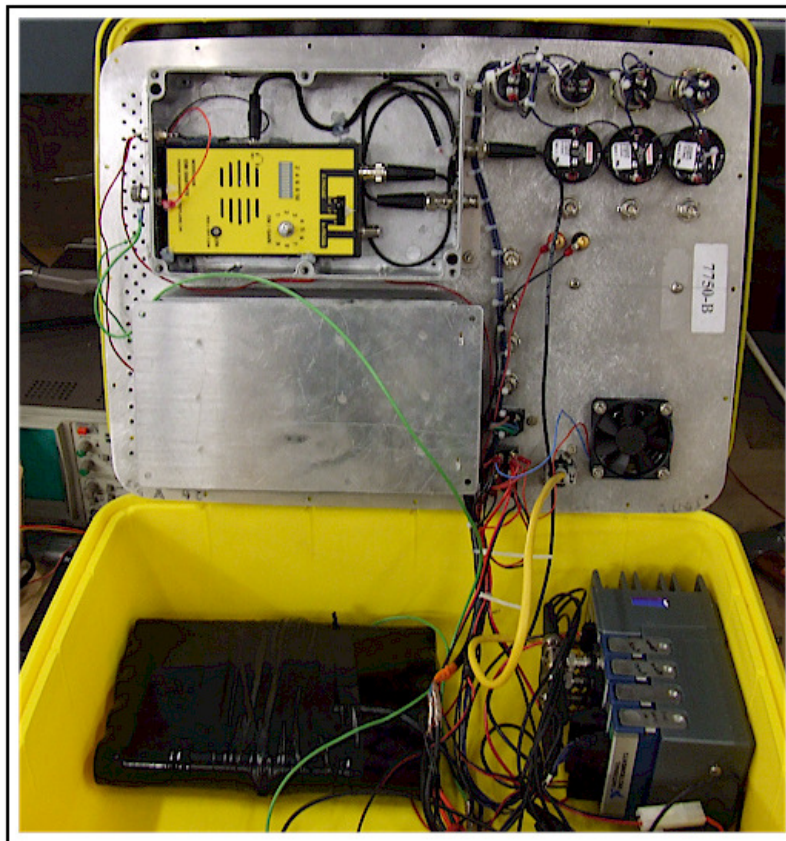


Figure 31. Physical Inside Layout of Arc Detection System

Shown in Figure 32, the sensor head is constructed of 6 inch PVC piping accessories. Internally, instead of using the standard whip antenna with the e-field meters, a strip of copper tape was used instead for each meter; low and high frequency. The whip antenna was more

directional; however, this application needed a more of an omnidirectional antenna to detect from any direction. Also, three custom magnetic rod antennas were constructed and arranged in a additive multi-axis configuration in order to maximize effectiveness in sensing the magnetic field from the cables in the manhole. This complete sensor pod is connected to the main system through 30 feet of signal cable, which allows for easy placement within the manhole vault.

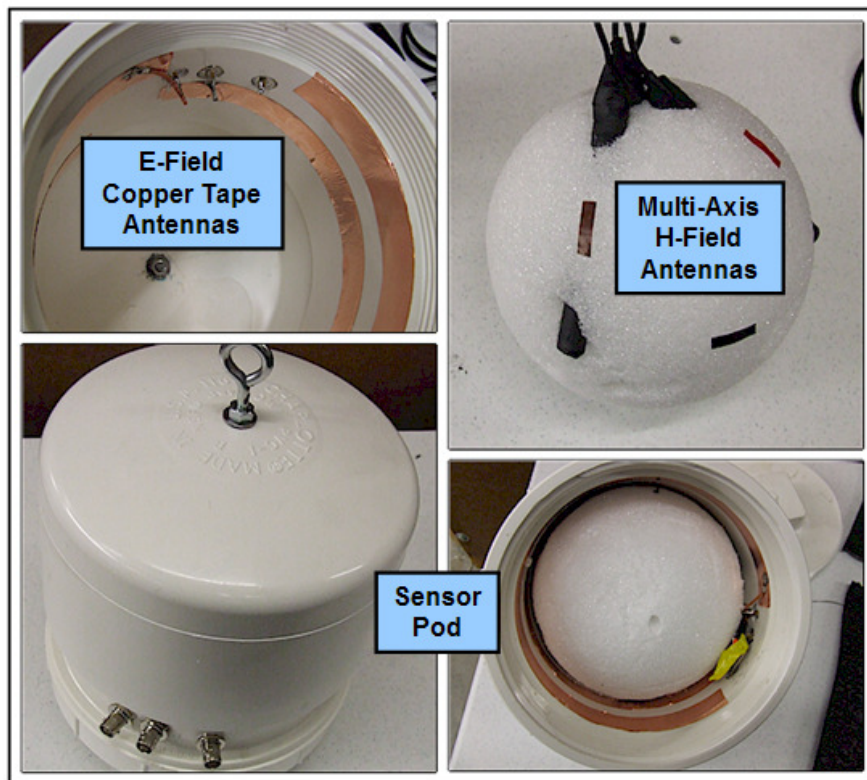


Figure 32. Sensor Head Layout with H-Field and E-Field Antennas

CHAPTER 4

RESULTS AND DISCUSSION

The prototype unit has been coined as the manhole arc recognition system or simply the MARS unit. Following along in Figure 33, the top portion of the unit, label A, has a on-off switch, ethernet port for communicating with the DSP system, a cooling fan, and battery charger connection. The unit can be completely charged in 1 hour and last up to 5 hours of operation before needing recharged. Label B is pointing to four output signals from the sensors that can be used to connect to a data acquisition system and record raw data. Label C is pointing to the sensor pod connections. Label D is the piezo alarms, with a low, medium, and high tone. Corresponding to those tones are three lights, label E, with the same level of alarms for visual indication. The green light is a system status light that communicates whether the system is running, and blinks a certain patterns for different messages. For example, if the magnetic sensor is not placed close enough to a conductor to pick up a signal, the light blinks on and off at a 1-second interval.

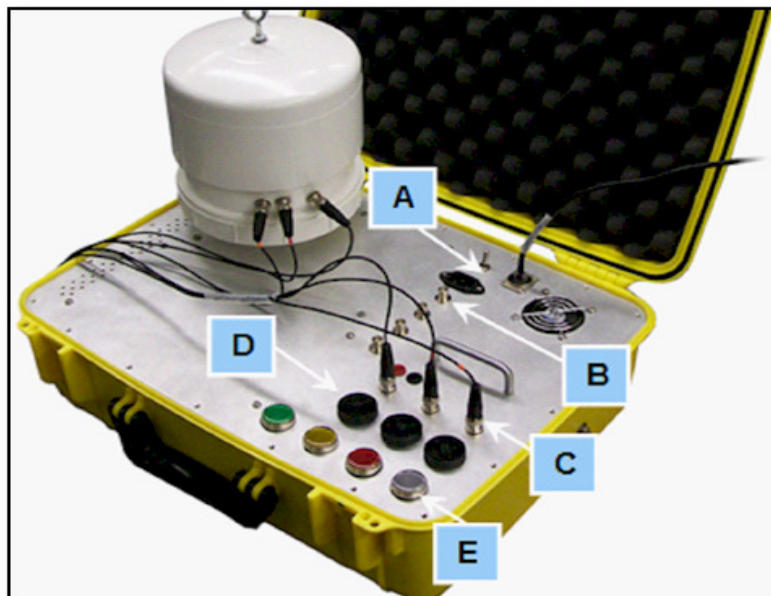


Figure 33. The Manhole Arc Recognition System (M.A.R.S.)

Lab Testing

Before field use the MARS system was put through several lab test to verify operation and ability to distinguish between arcs and other noise sources. In a field environment, an electrical manhole can have on average 50 to 300 amps of load current flowing through the lines. Before an arc develops into a high current fault, the current can range anywhere from milliamps to a few amps. This means the signature of these arc events are mixed with the normal clean currents that are 10's to 100's of times greater. To simulate this environment a test was constructed, as shown in Figure 34. The setup consist of two rooms; one is a screen room that houses the arc source, the other is a shielded enclosure that houses the sensor pod.

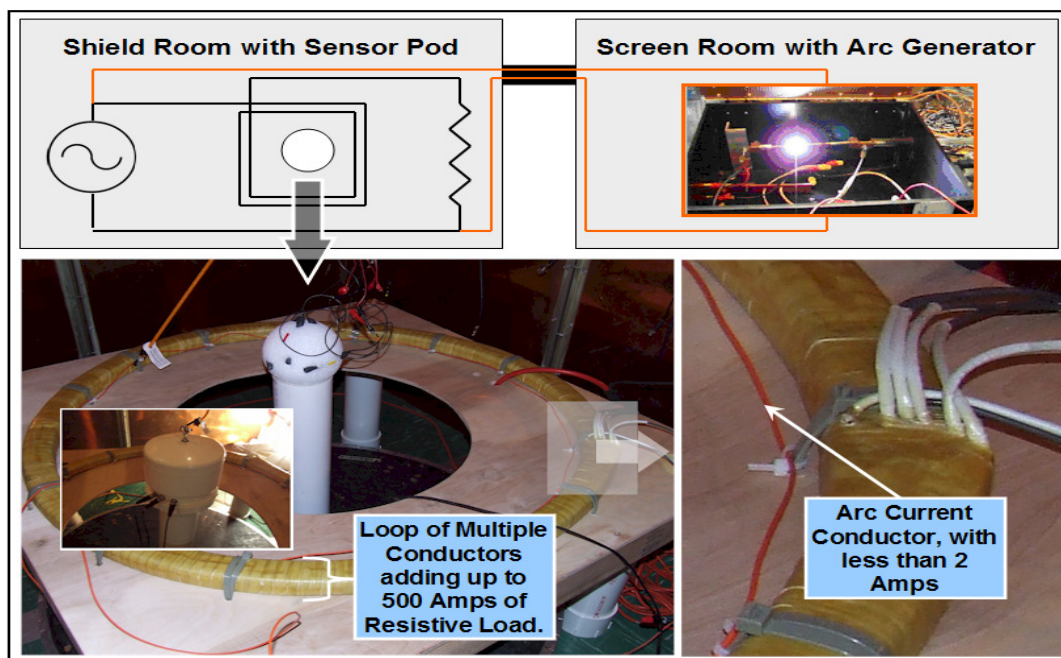


Figure 34. Lab Setup Simulating Manhole Ambient Currents with Arc Current

The two rooms are connected by a 1/2-inch, schedule-40 metallic conduit. Power is supplied from a filtered source to a resistive bank in the shielded enclosure. In parallel to this load, with the wires passed through the conduit, is the arc source. Around the sensor are multiple turns of wire for the resistive load, and one wire for the arc source. This will allow the sensor to see up to 500 amps of resistive current and less than 2 amps in arc current. Shown in Figure 35, is the baseline resistive signature from the h-field sensor.

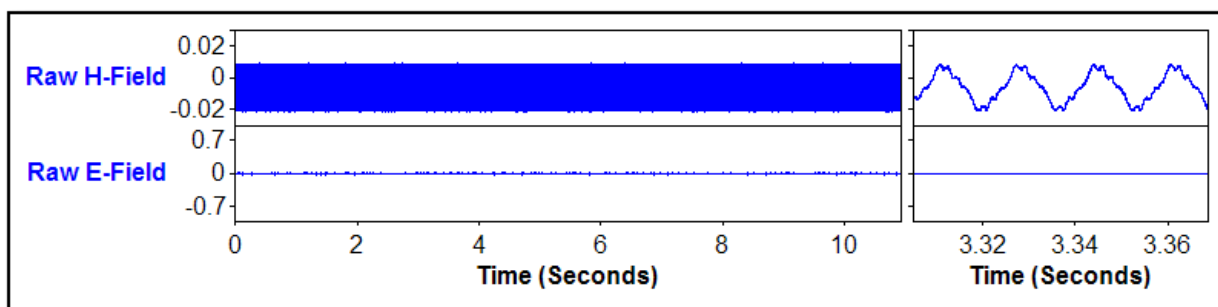


Figure 35. Baseline H-Field and E-Field Measurements from Lab Manhole Test

For this test setup other loads that have potential to give false positives can replace the arc load. For comparison each algorithm was processed for a neon sign with switch-mode power supply, a pulse-width-modulation motor drive, and an SCR-controlled handheld drill. In Figure 36 the current signatures are shown for each load as well as the raw h-field and e-field measurements.

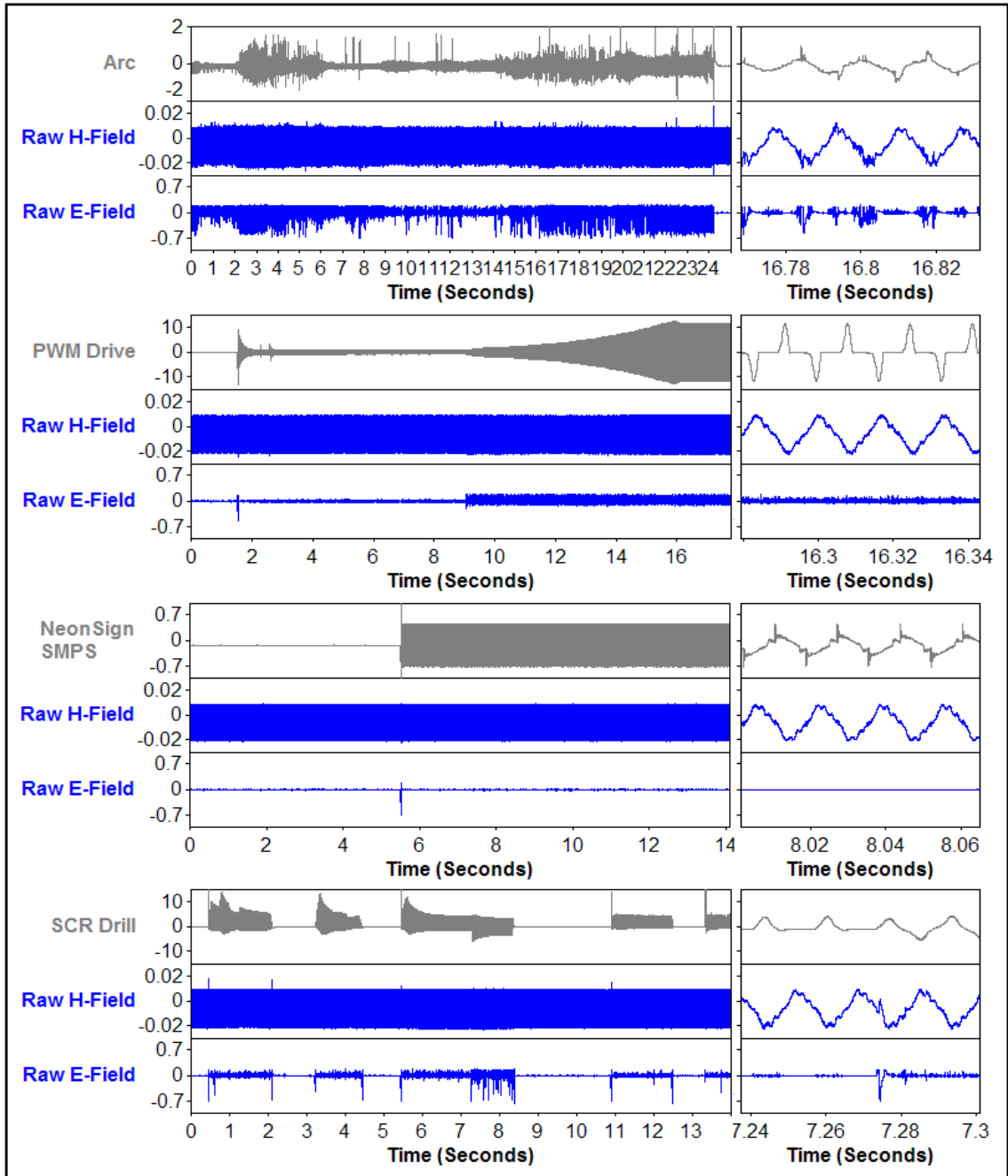


Figure 36. H-Field and E-Field Output from Arcing and False Positive Loads

Each of the following algorithm graphs shows changes (Δ) or values in a 100-millisecond window. The relative amplitudes show how the algorithms responded to the arcing. The limits and pulse have yet to be defined, as further field studies will be needed to estimate for those values.

Crest Factor Algorithm Results

Shown in Figure 37 are the test results from the MARS crest factor. The amplitude is not as high as was analyzed with the previous waveform. This is due to the arcing being mixed with the large resistive current. In the raw h-field, the change in the wave shape is subtle. For this reason level triggering may not be feasible; however, the derivation change may still be a viable measurement for crest factor. In comparison the arcing is easily distinguishable from the other loads

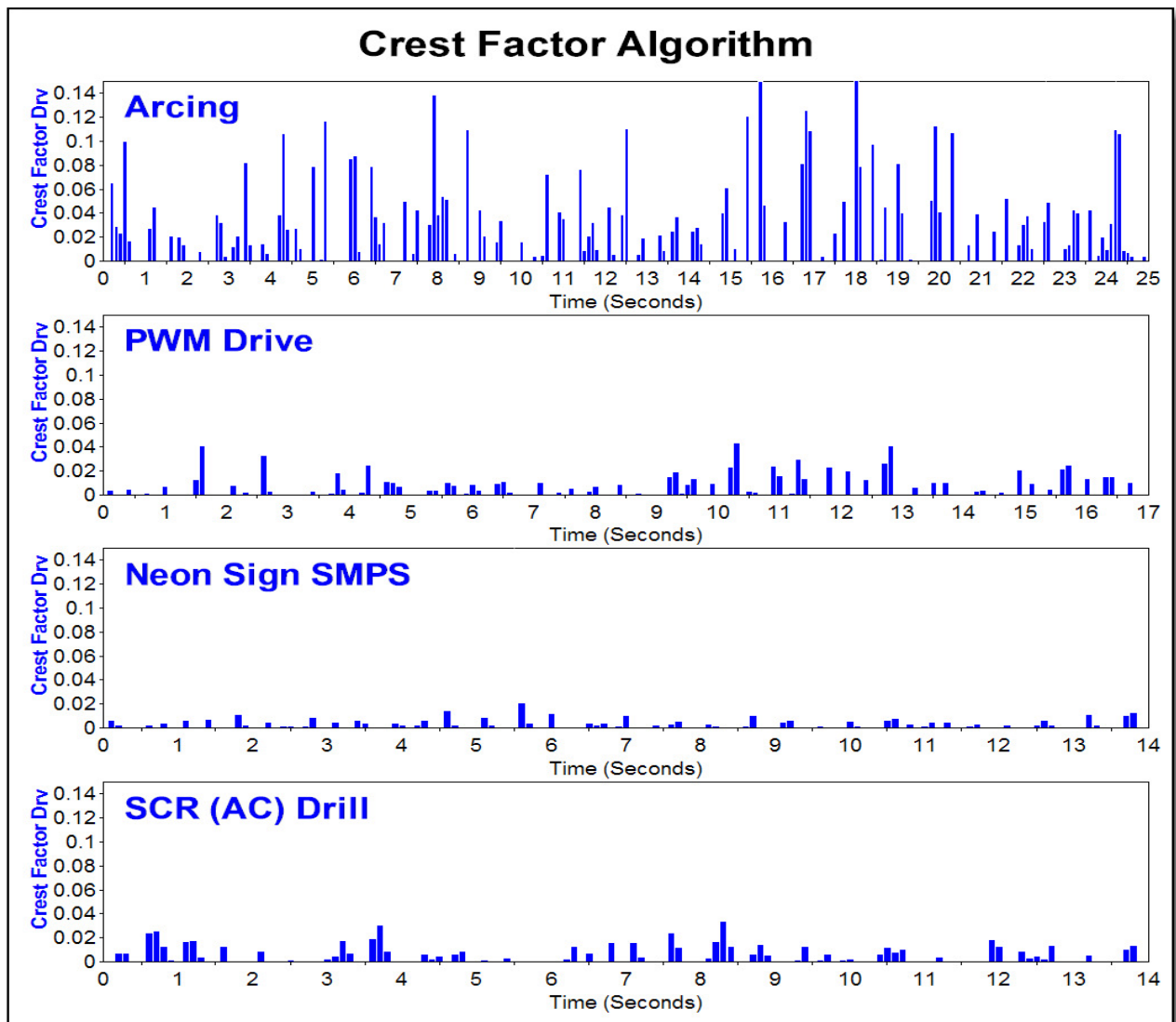


Figure 37. Crest Factor Algorithm Test Results

Differentiation Algorithm Results

All the loads had a high frequency content to their current signature, which the initial 3rd derivative calculation picks up on. However, the arcing waveform was the only load that was sporadic. After sampling the max of the derivative, the additional derivative filters any steady-state high frequency content that we see in the other loads. The arcing high frequency content is continually changing as illustrated in the differentiation algorithm shown in Figure 38.

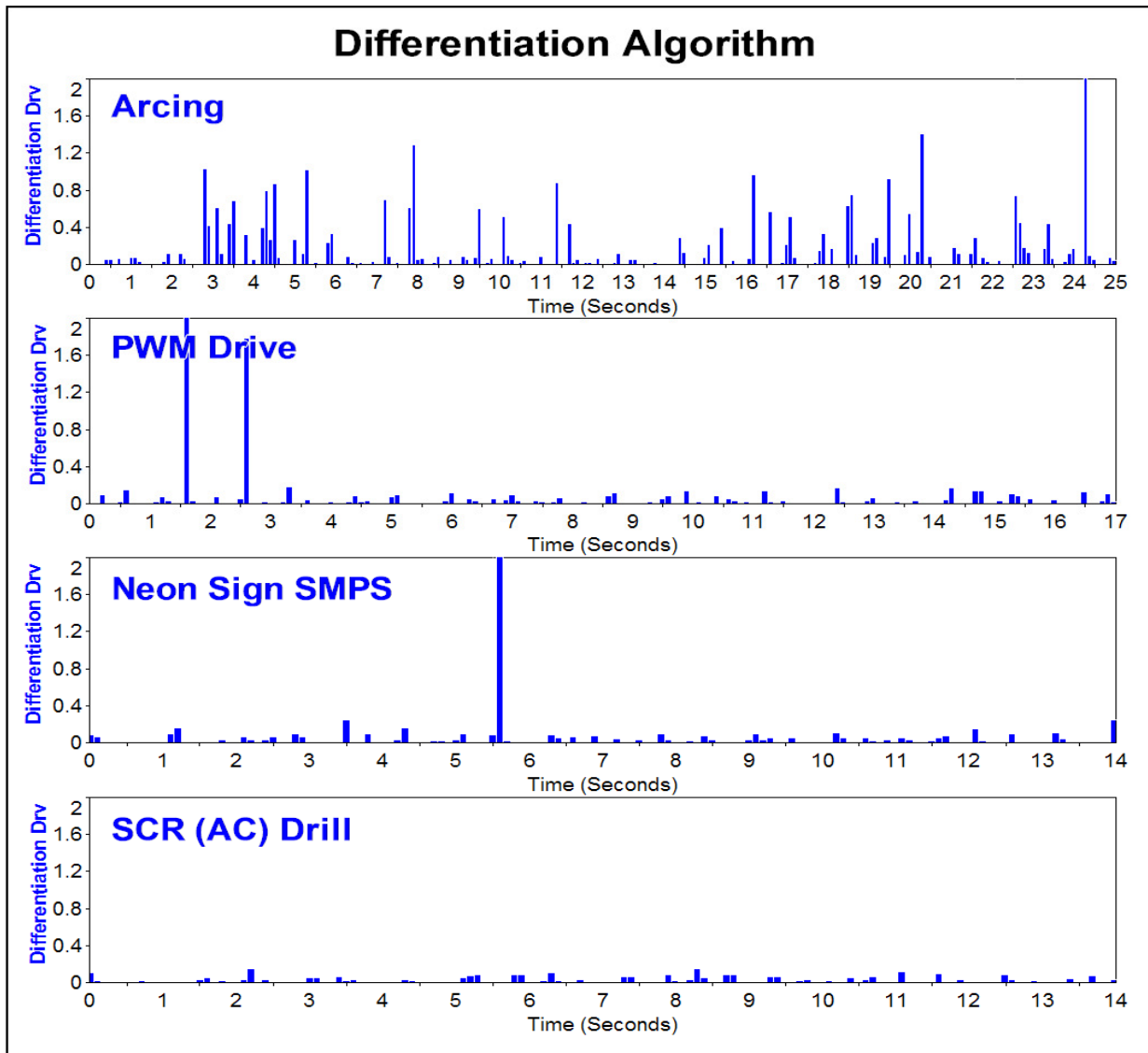


Figure 38. Differentiation Algorithm Test Results

Interharmonics Algorithm Results

Most 60Hz loads do not contain significant amounts of interharmonics. Usually only continually changing loads like arcing produce the unsymmetrical currents that make up interharmonics. For this test the operation of the drill was another load that was continually changing as it was being used. The initial currents, refer to previous Figure 36, only conducted half-cycles, and then when the trigger was let go, the drill would generate some counter electromagnetic force currents as it was spinning down. As shown in the results below in Figure 39, this could potentially trigger a false positive alarm.

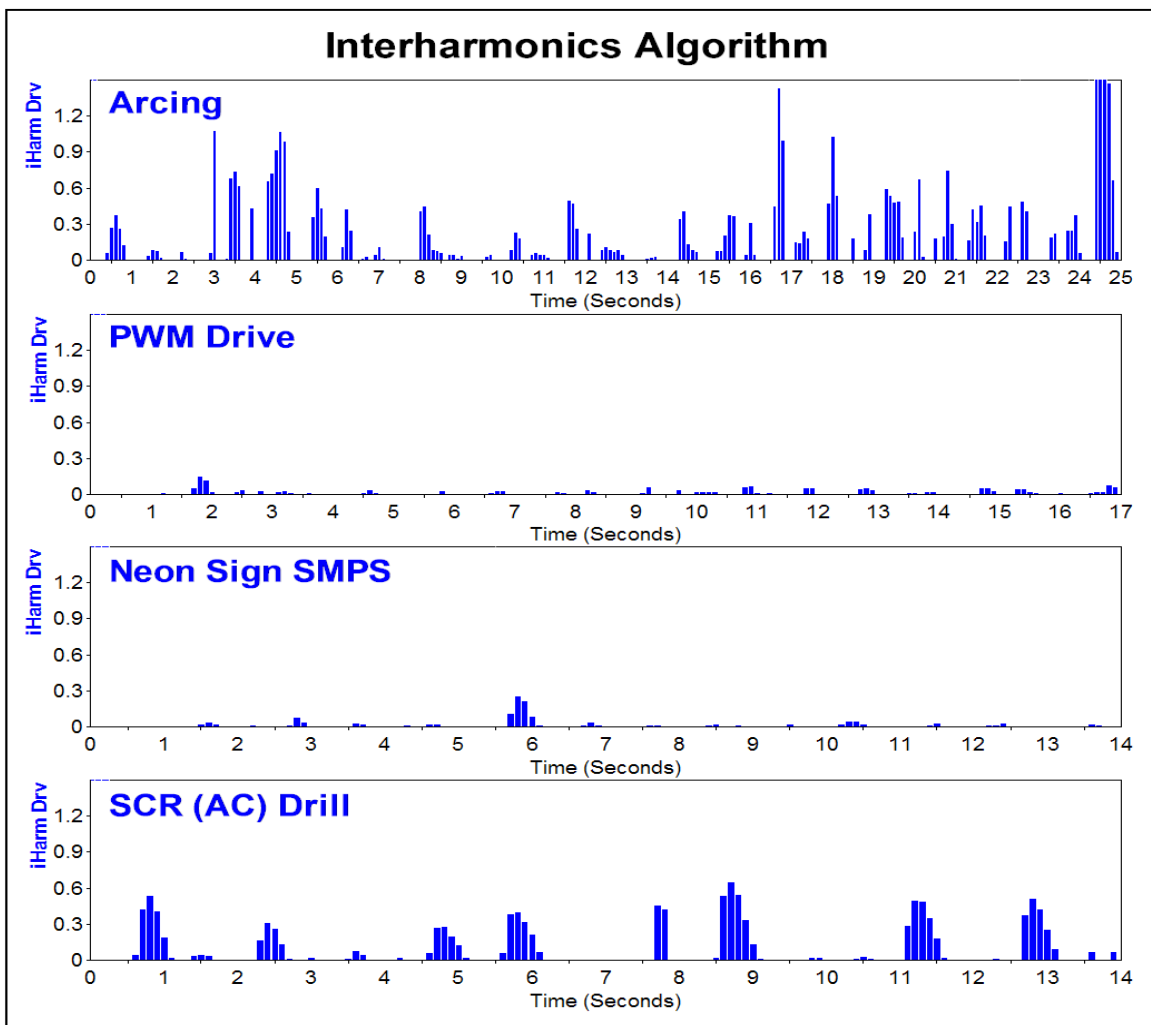


Figure 39. Interharmonics Algorithm Test Results

120 Hz Repetition Algorithm Results

As can be seen in Figure 40, only the arcing showed a 120 Hz repetition output. It was suspected that the neon signs high frequency output at the top of each cycle would trigger this as a false positive; however, being that the SMPS frequency is lower than the arcing frequency, it seems the lower frequency resulted in a lower derivative magnitude that did not trigger the limit set by the arcing.

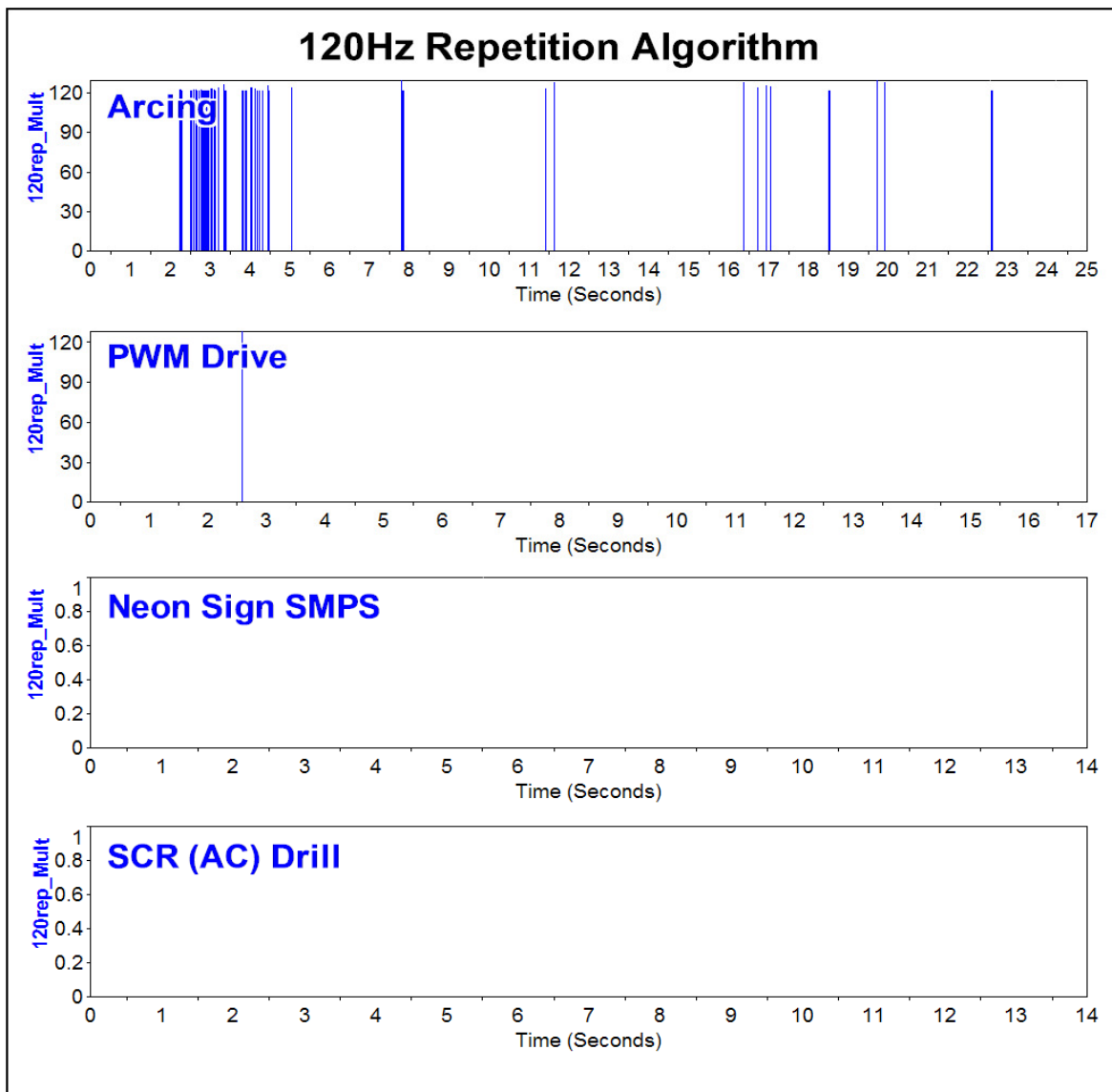


Figure 40. 120 Hz Repetition Rate Algorithm Test Results

120 Hz Demodulation Algorithm Results

Looking at the raw data in Figure 41, we know that the e-field meter produced an output for arcing, the PWM drive, and the drill. This means it detects some noise in the MHz range. However, only the arcing shows a signal-level significant to trigger an alarm. There are two contributing factors in this algorithm. One is using the demodulation from the e-field meter to eliminate steady noise given from the PWM drive. And even though the drill uses AC, the motor inside the drill is DC. Just as we seen with a DC drill, the arcing does not give a demodulated 60Hz multiple signature that this algorithm looks for as a trigger.

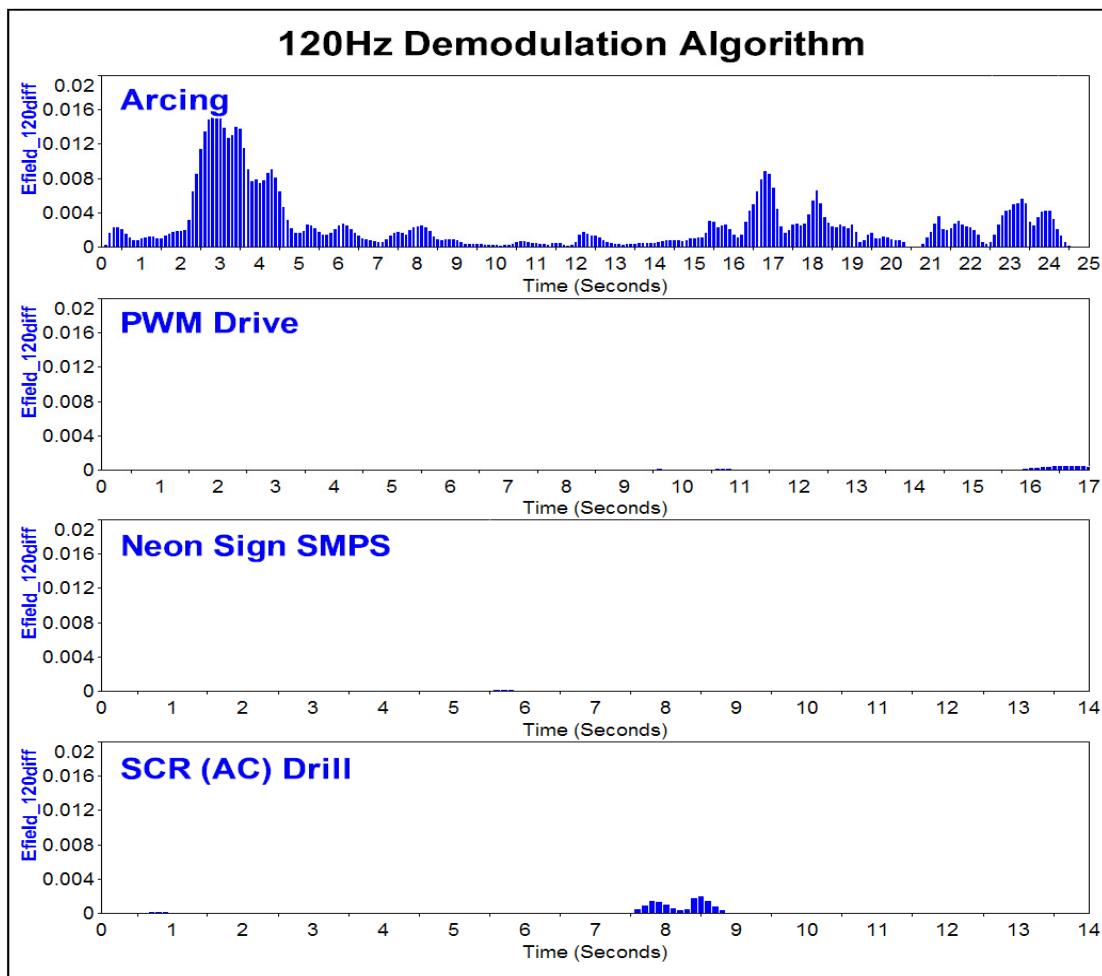


Figure 41. 120 Hz Demodulation Algorithm Test Results

180 Hz Demodulation Algorithm Results

As can be seen in Figure 42, the 180 Hz demodulation algorithm gives the same result as the 120 Hz version. Future studies may be conducted to see which is more conclusive for arcing; however, in this test the 120 Hz version give better results.

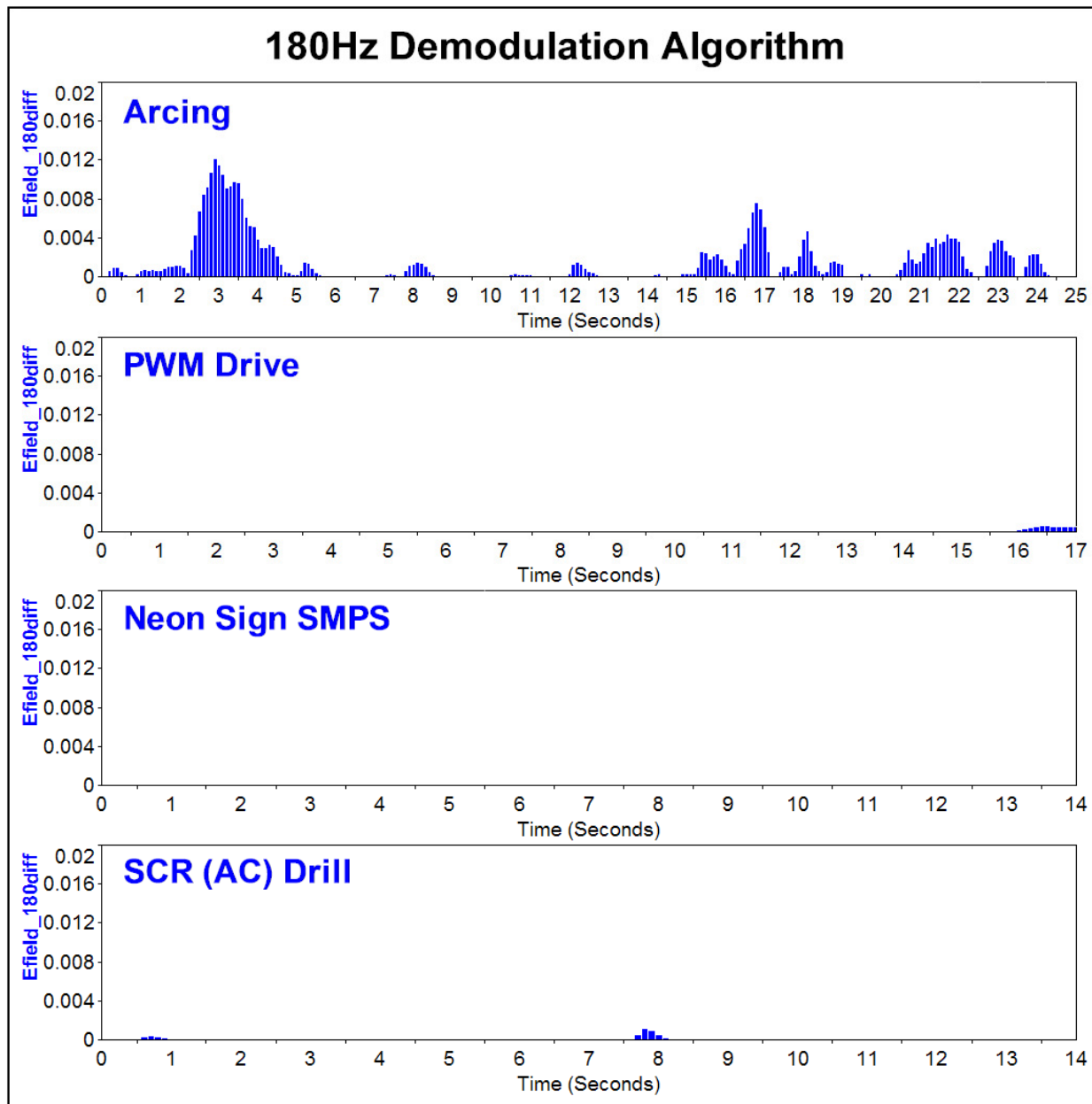


Figure 42. 180 Hz Demodulation Algorithm Test Results

Sporadic Efield Algorithm Result

Leaving out the waveform signature, the sporadic algorithm simply looks for sudden changes. As can be seen in Figure 43, both the arc and drill would trigger this alarm. As with the high frequency h-field, the dynamic use of a drill leads to the continuous change in the motors arcing. This demonstrates that in a field environment, we may measure an input to a facility that has many dynamic type loads that may easily give a false positive for this algorithm and the differentiation algorithm.

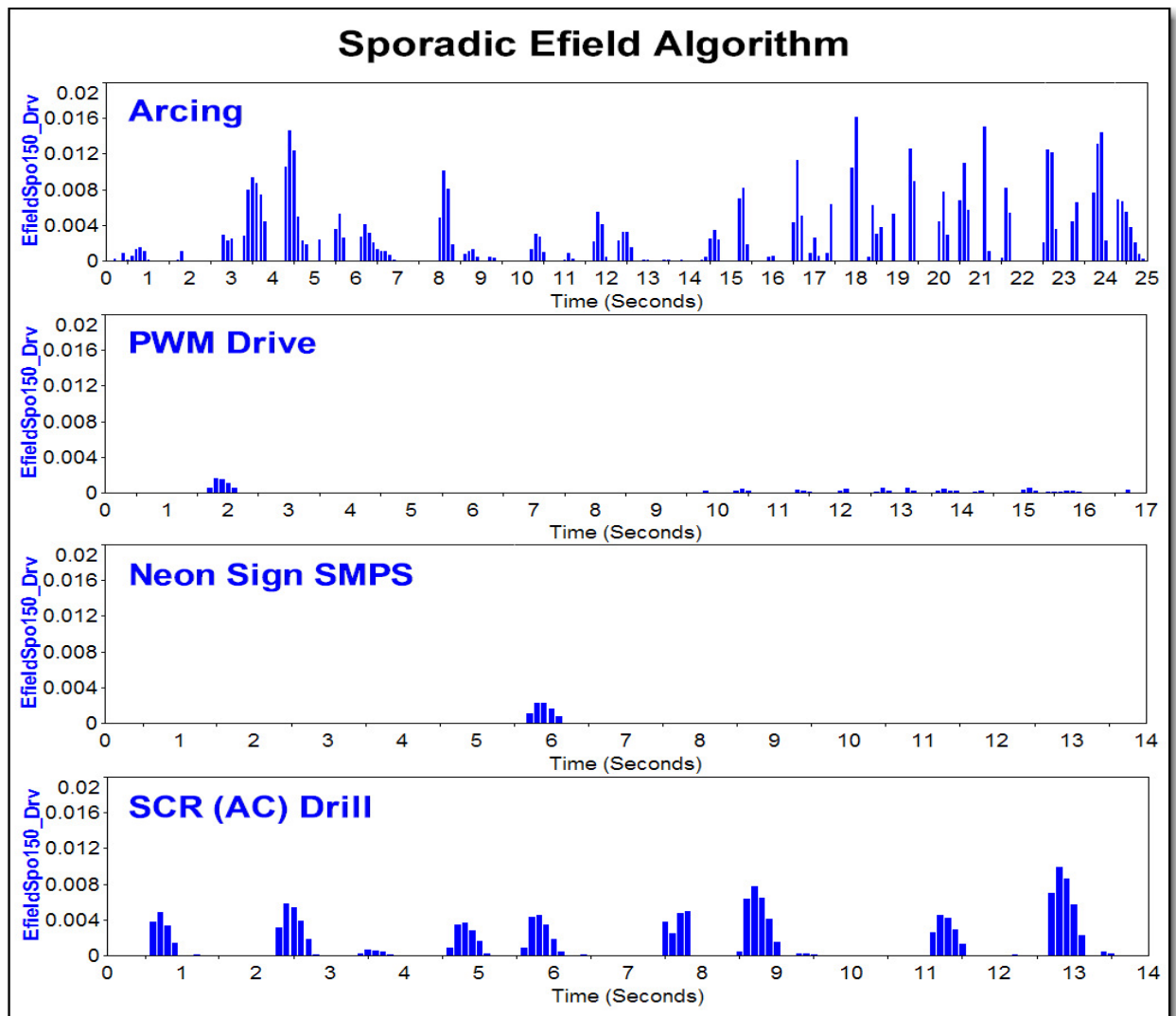


Figure 43. Sporadic E-Field Algorithm Test Results

Field Testing

As this thesis is being written the MARS development prototype is being used in the field and collecting data, as can be seen in Figure 44. The main objective at this point is to collect enough background data from this environment in order to fine tune the algorithm trigger levels and trigger counts.

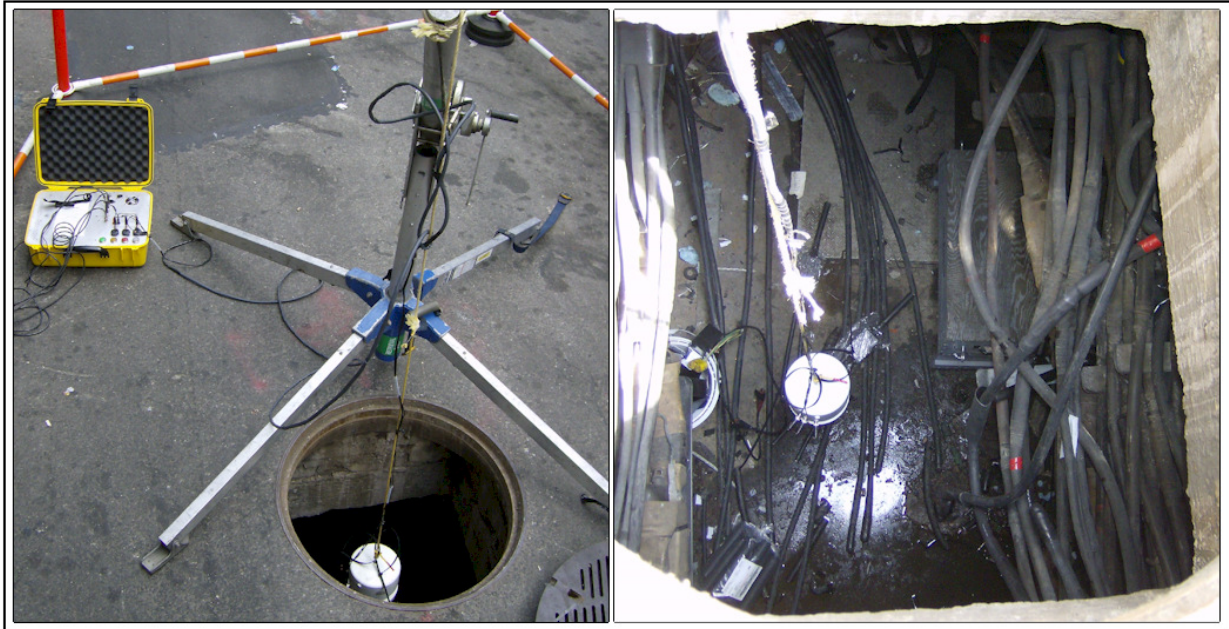


Figure 44. MARS System Used in a Field Environment

At the same time the system is being subjected to numerous loads that have potential for false positives. One site has a subway that is 30 feet above ground from the manhole. This subway uses a DC third rail to power its trains. The connection between the rail and the train can intermittently produce arcing as it moves along the tracks. The electric utility reported that the MARS system was triggering low and medium alarms as the trains passed overhead. The data collected by the utility were analyzed, and as can be seen in the frequency and spectrogram plot in Figure 45, the signature from the e-field meter shows sporadic arcing; however, because there

is not any 60 Hz multiple dominant in the signature, we can rule that this is indeed a false positive.

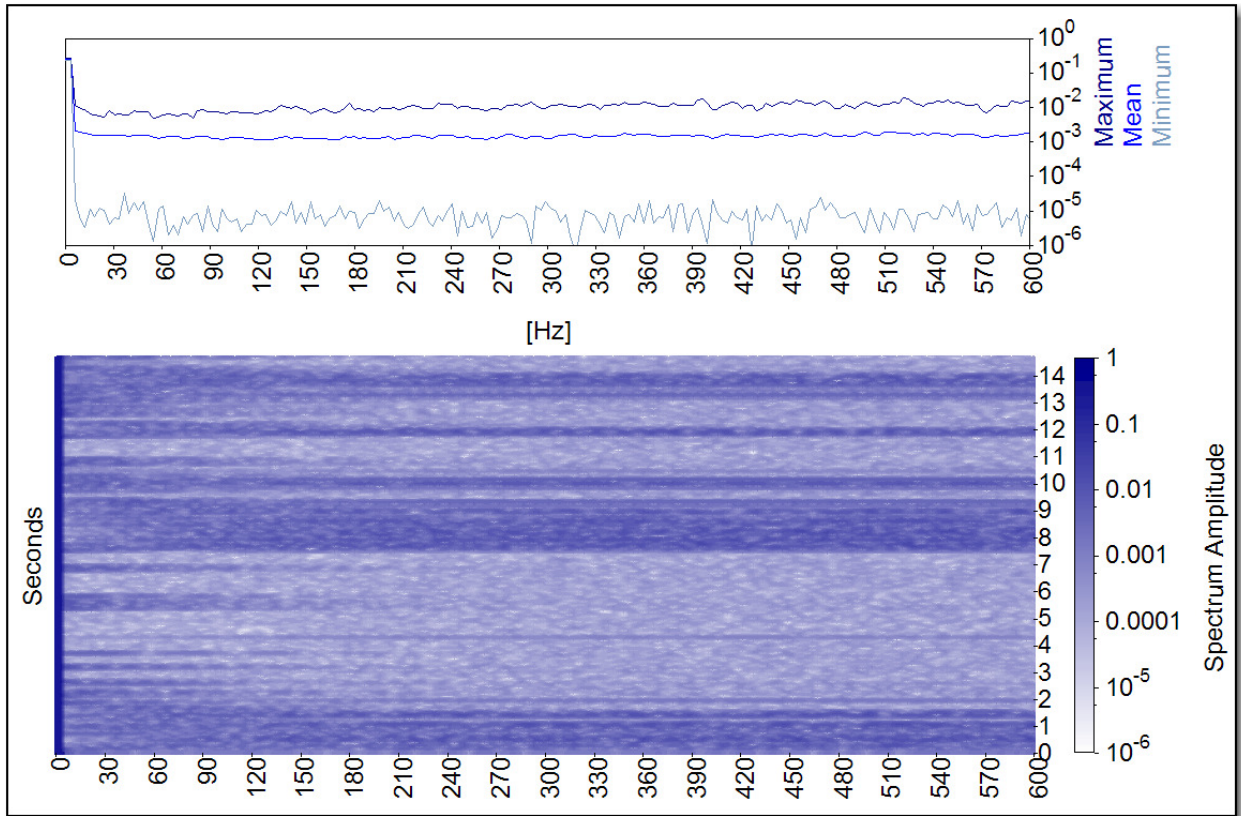


Figure 45. E-Field Frequency Analysis of Above Ground Subway with Arcing from DC Rail

CHAPTER 5

CONCLUSION

Arcing in an underground manhole environment can lead to serious damage or even fatalities. For several decades manufacturers, researchers, and utilities have been tackling how to detect arcing before it evolves into a high current fault. Detection has been proven with various methods; however, distinguishing them with other loads and basic grid operation false positives has not been proven. Based on literature research, using a non-contact approach with both electric field and magnetic field is a unique approach for underground system measurements. As the data have shown, each algorithm has a potential for detecting false positives. However, combining each set of algorithms from magnetic and electric fields helps eliminate false positives and significantly increases the confidence in detecting actual arcs from an electrical fault.

Future Recommendations

The lab and field results are very promising. Still, the system has only been exposed to a few loads with potential for false positives. Field testing will reveal future loads, just as it revealed the subway system as a false positive. As each load is identified, changes may be made to each algorithm. In addition, some extra algorithms may not be needed. This will help reduce processing power as well as size of the system. Once the algorithms are decided, future plans involve incorporating these algorithms into a smaller digital signal processor or possibly an analog equivalent circuit that can be placed in a hand-held device as depicted in Figure 46.

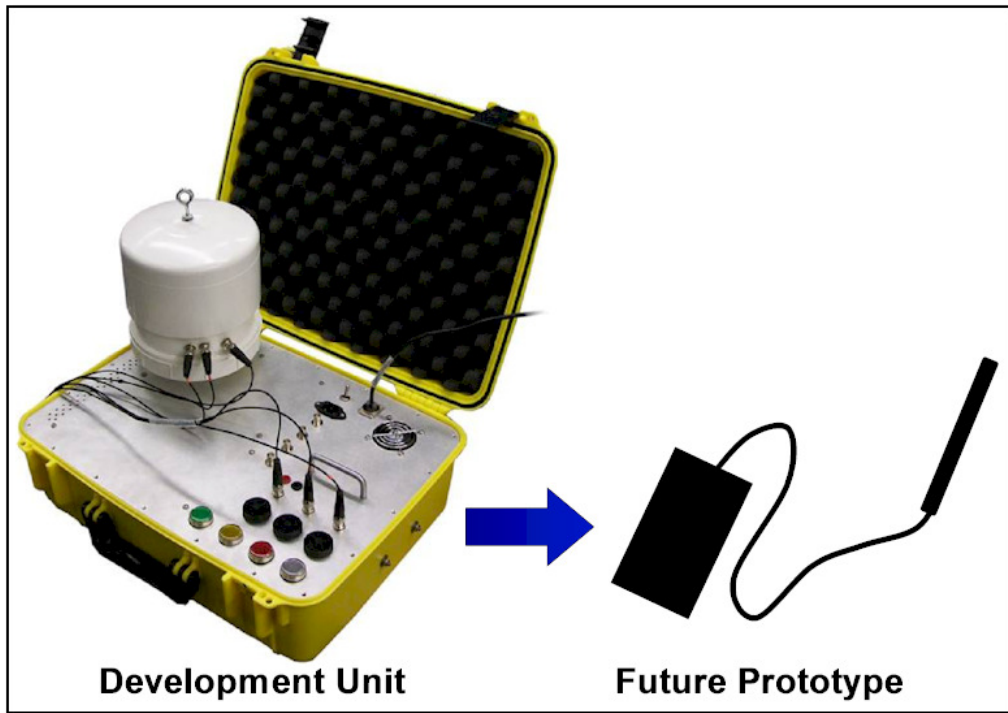


Figure 46. Illustration of Future Goal for Smaller Hand-Held Arc Detection Unit

REFERENCES

- Charytoniuk, W., Lee, W.J., Chen, M.S. Cultrera, J., & Maffetone, T. (2000). Arcing fault detection in underground distribution networks – feasibility study. *IEEE Transactions on Industry Applications*, 36, 1756-1761.
- EPRI Report EL-2430, (1982). High impedance fault detection using third harmonic current. Palo Alto, CA: *Electric Power Research Institute*.
- Kim, C. J., & Russell, B. D. (1988). Harmonic behavior during arcing faults on power distribution feeders. *Electric Power System Research*, 14, 219-225.
- Kim, C. J., Russell, B. D., & Watson, K. (1990). A parameter-based process for selecting high impedance fault detection techniques using decision making under incomplete knowledge. *IEEE Transactions on Power Delivery*, 5, 1314-1320.
- Kim, C. J., & Russell, B. D. (1995). Analysis of distribution disturbances and arcing faults using the crest factor. *Electric Power Systems Research*, 35, 141-148.
- Kim, C. J. (2009). Electromagnetic radiation behavior of low voltage arcing fault. *IEEE Transactions on Power Delivery*, 24, 416-423.

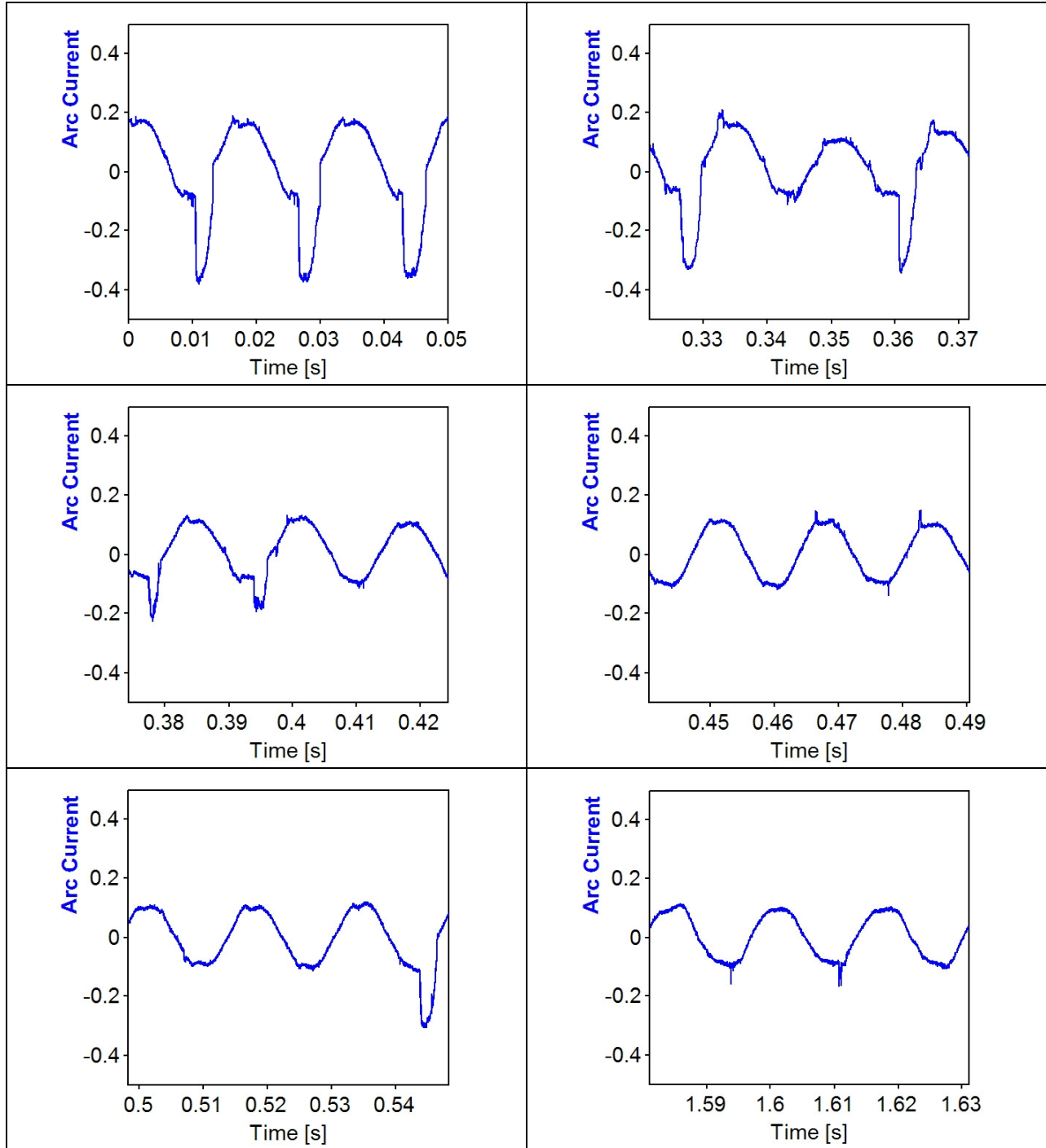
Land, H. B., Eddins, C. L., & Klimek, J.M. (2004). Evolution of arc fault protection technology at APL. *Johns Hopkins APL Technical Digest*, 25, 140-153.

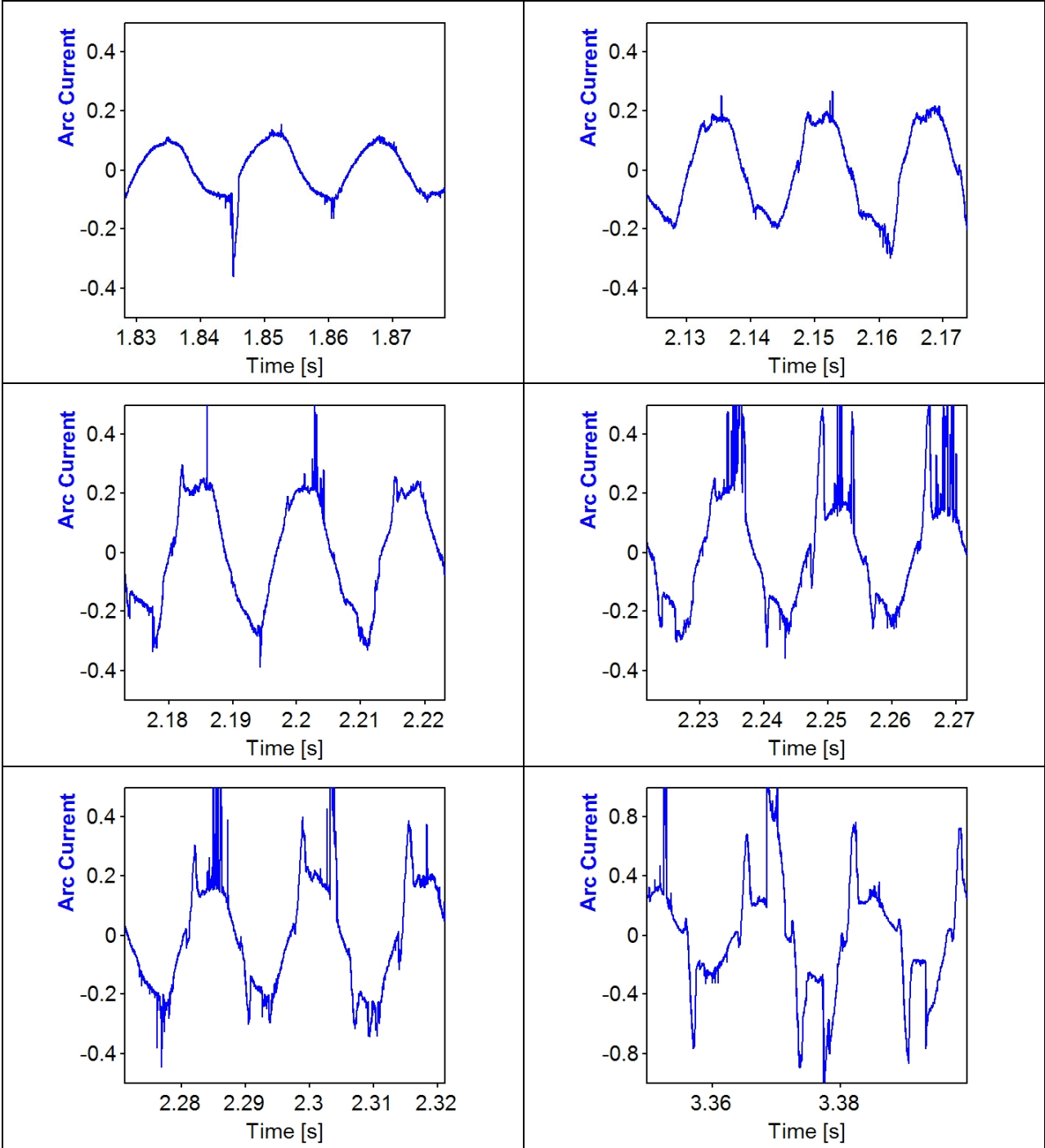
Lee, D.A., Trotta, A.M., & King, W.H. (2000). New technology for preventing residential electrical fires: Arc-fault circuit interrupters. *Fire Technology*, 36, 145-162.

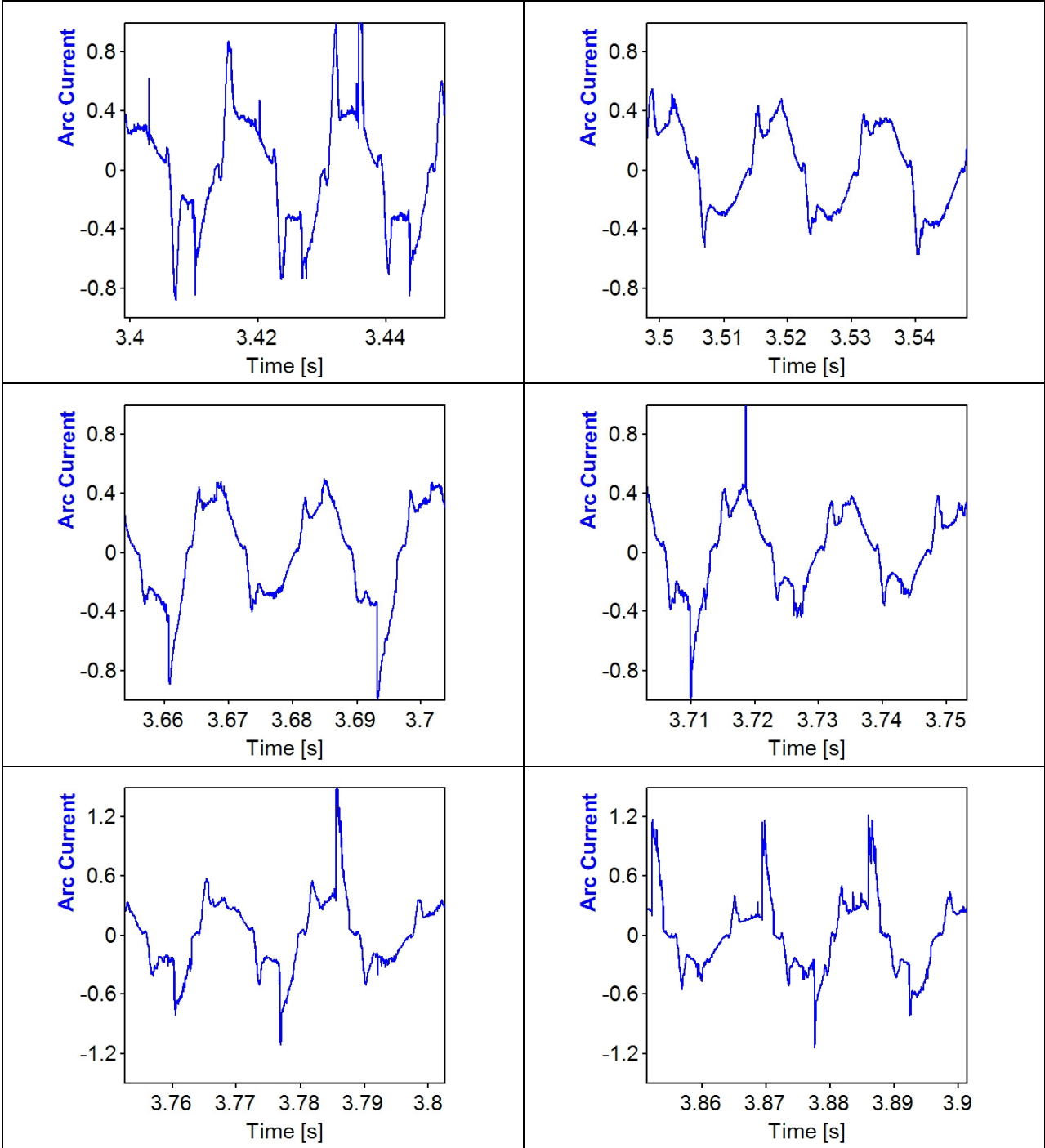
Rogers, J.H., & LaRue, P. (1995). RF arc detection using harmonic signals – Fusion engineering. *16th IEEE/NPSS Symposium*, 522-525.

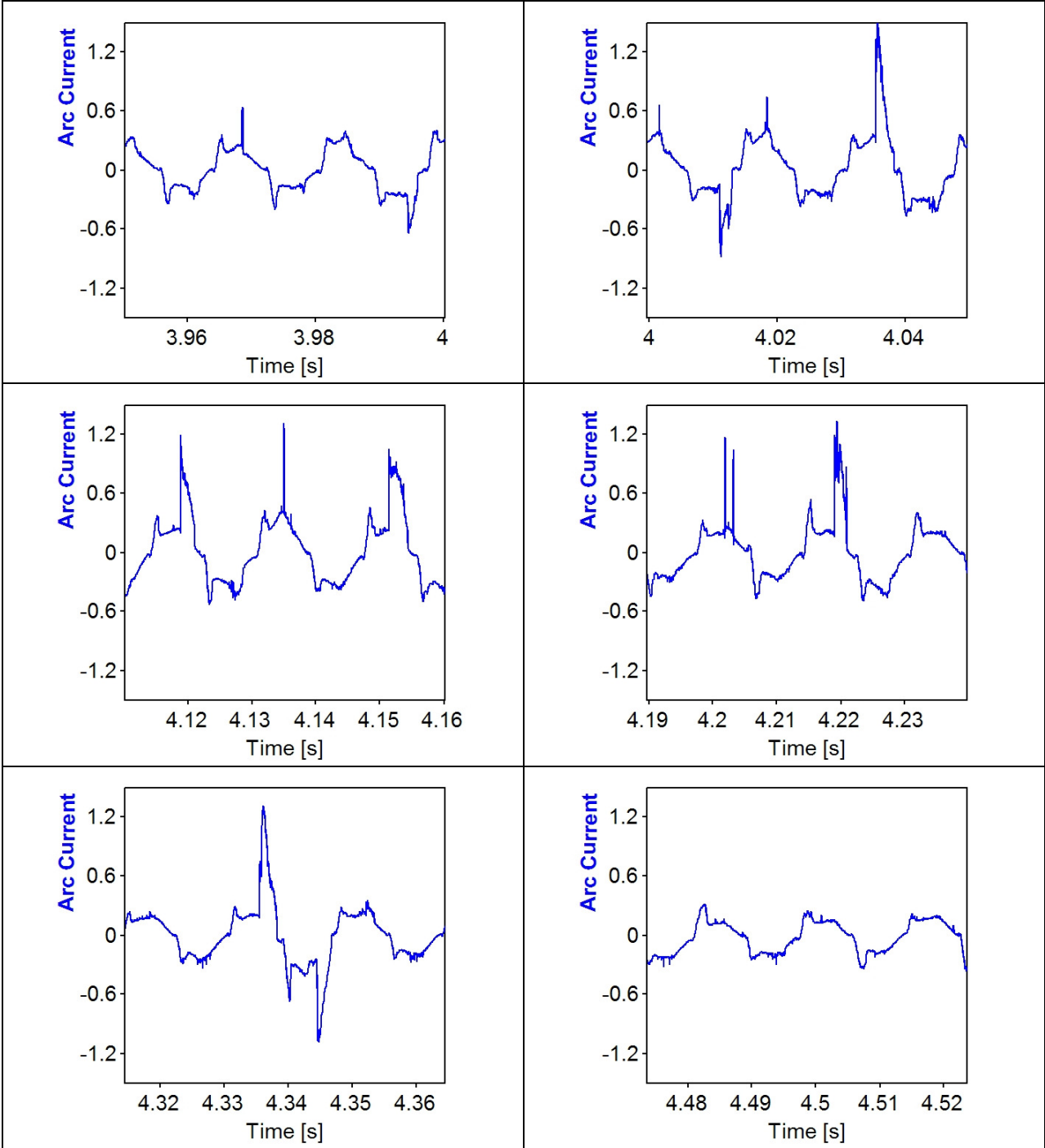
APPENDIX

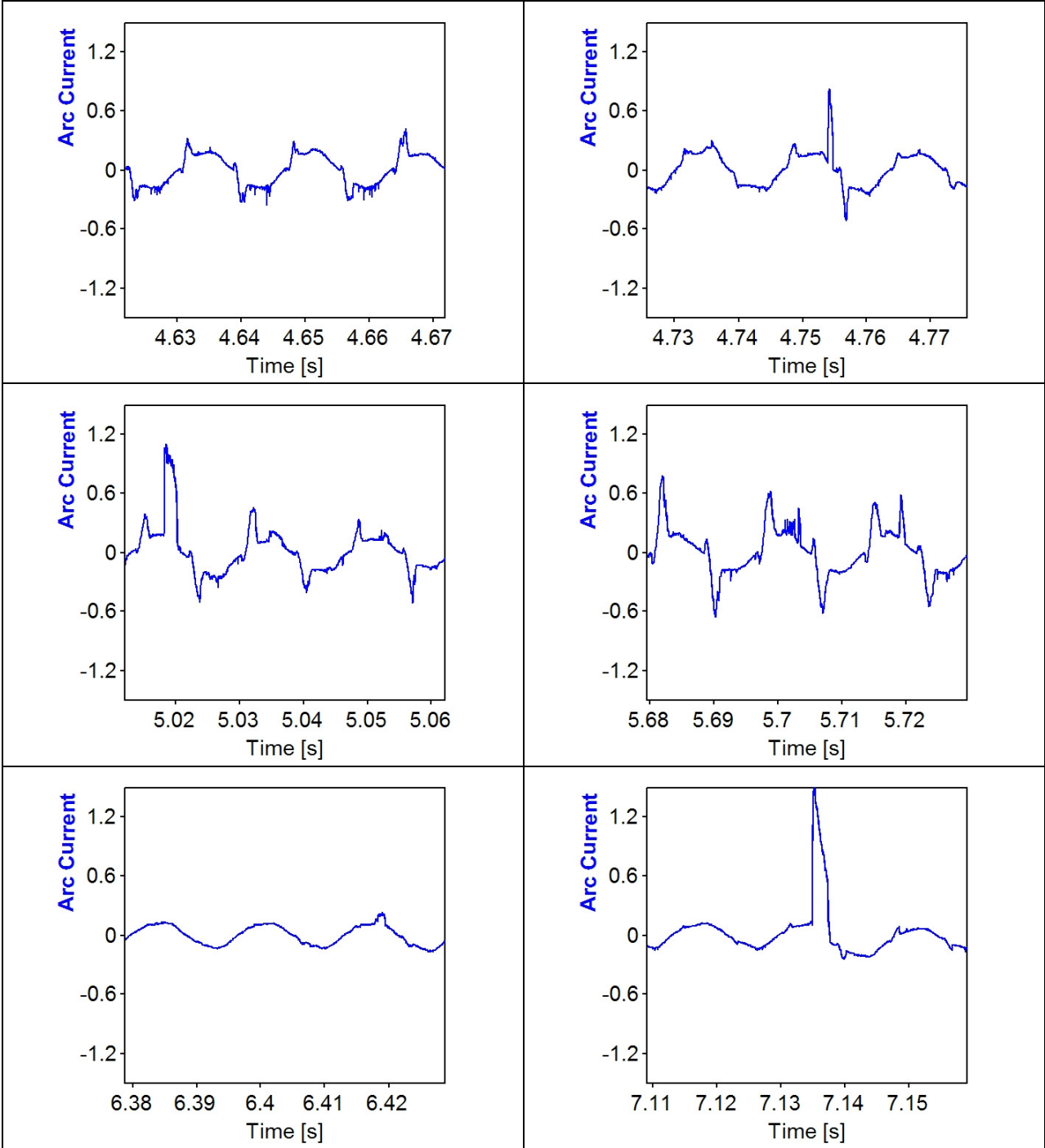
Series Sequence of Waveforms from a Single Arcing Event

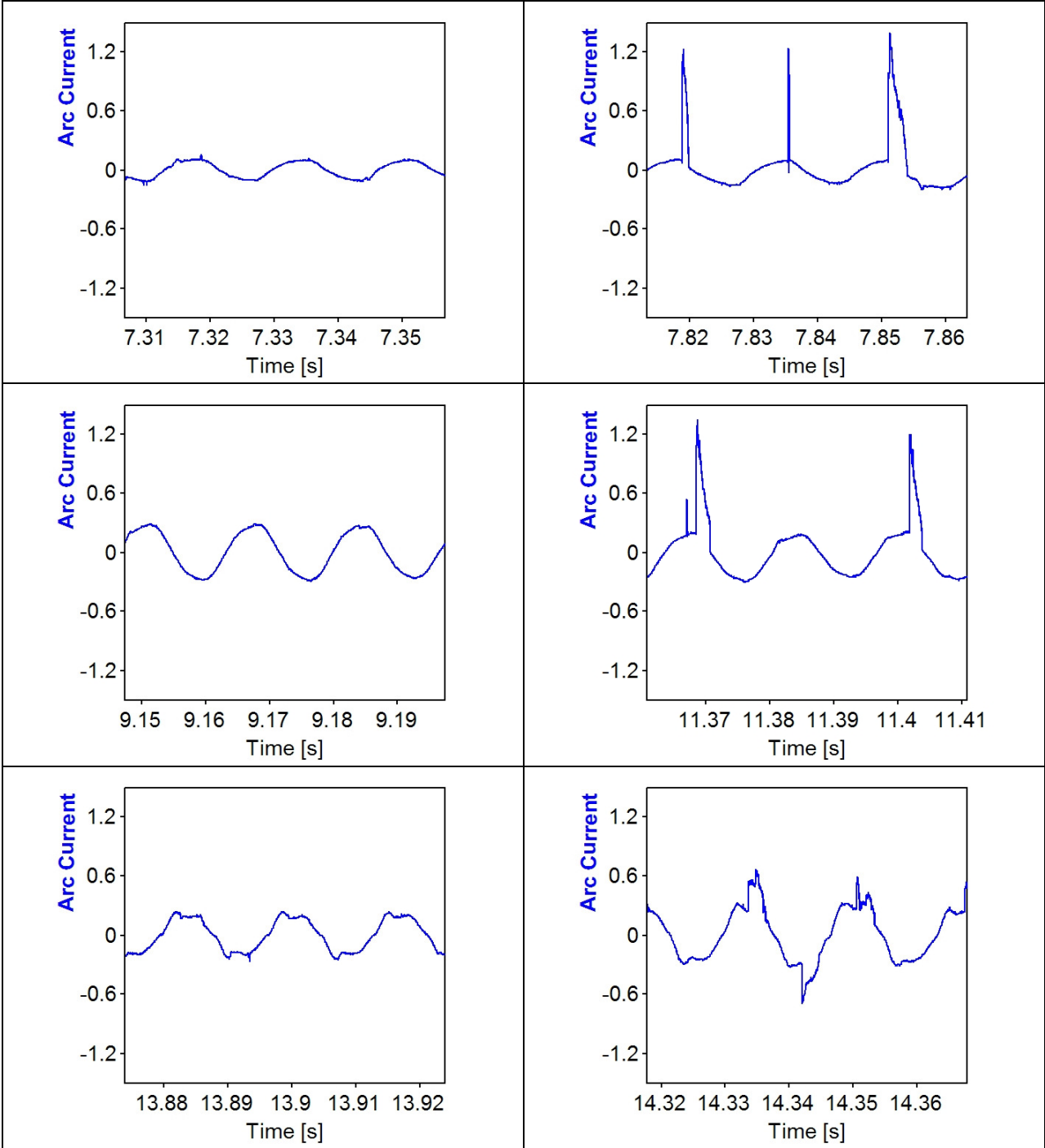


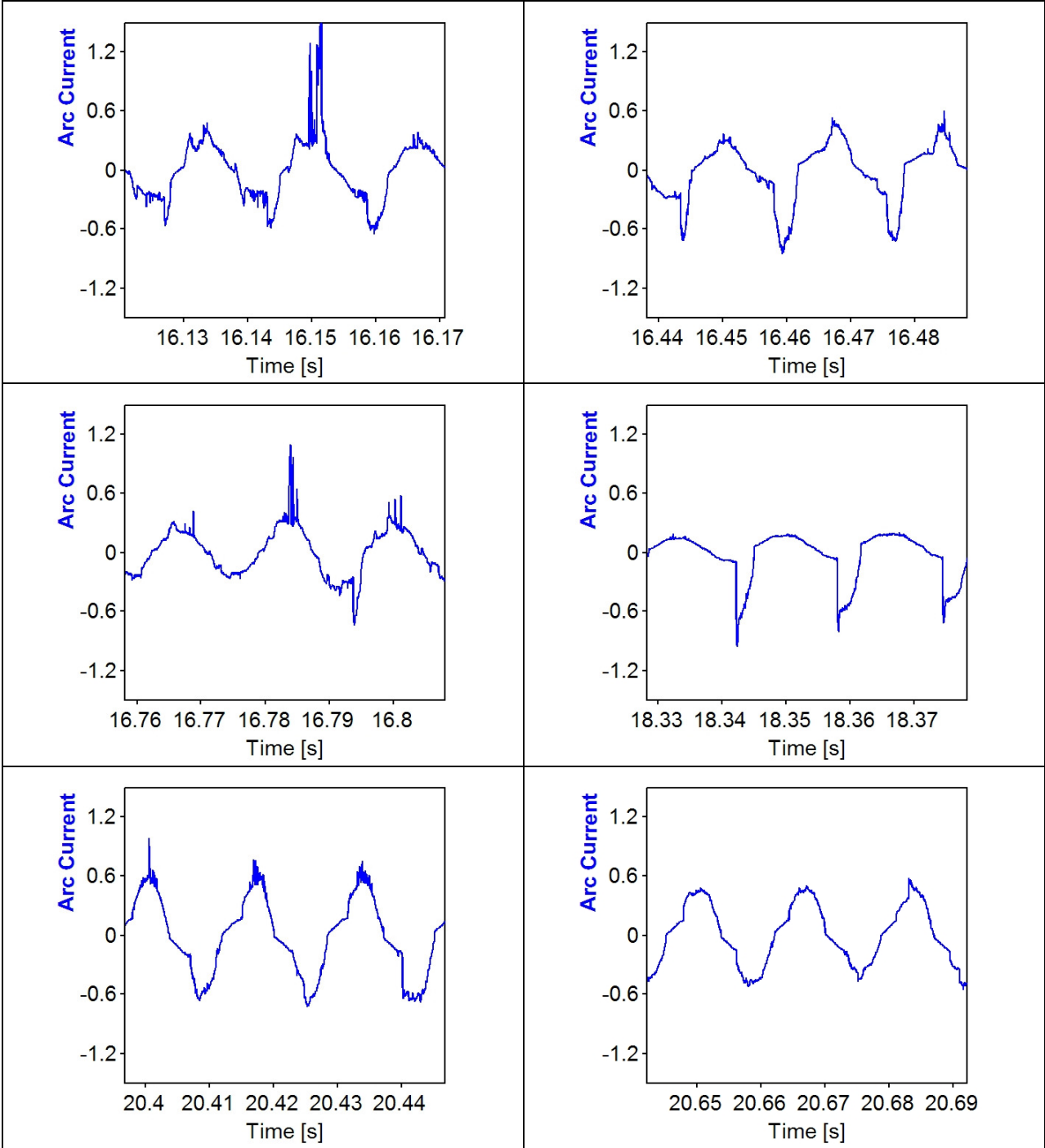












VITA

THOMAS ARTHUR COOKE

Personal Data:

Date of Birth: December 2, 1969

Place of Birth: Knoxville, Tennessee

Marital Status: Married

Education:

A.A.S. Electronics Engineering Technology, Pellissippi State
Community College, Knoxville, Tennessee 1998

B.S. Electronics Engineering Technology, East Tennessee State
University, Johnson City, Tennessee 2008

M.S. Technology, East Tennessee State University,
Johnson City, Tennessee 2010

Professional Experience:

Project Engineer, Electric Power Research Institute, Knoxville,
Tennessee, 1997 to Present